Group theoretical approach to computing phonons and their interactions

Lyuwen Fu,[1,*] Mordechai Kornbluth,[2,†] Zhengqian Cheng,[1,‡] and Chris A. Marianetti[1,§]

[1]*Department of Applied Physics and Applied Mathematics, Columbia University, New York, New York 10027, USA*
[2]*Robert Bosch LLC, Research and Technology Center North America, One Kendall Square, Cambridge, Massachusetts 02139, USA*

Phonons and their interactions are necessary for determining a wide range of materials properties. Here we present four independent advances which facilitate the computation of phonons and their interactions from first principles. First, we implement a group-theoretical approach to construct the order $\mathcal{N}$ Taylor series of a d-dimensional crystal purely in terms of space group irreducible derivatives (ID), which guarantees symmetry by construction and allows for a practical means of communicating and storing phonons and their interactions. Second, we prove that the smallest possible supercell which accommodates $\mathcal{N}$ given wave vectors in a d-dimensional crystal is determined using the Smith normal form of the matrix formed from the corresponding wave vectors; resulting in negligible computational cost to find said supercell, in addition to providing the maximum required multiplicity for uniform supercells at arbitrary $\mathcal{N}$ and d. Third, we develop a series of finite displacement methodologies to compute phonons and their interactions which exploit the first two developments: lone and bundled irreducible derivative (LID and BID) approaches. LID computes a single ID, or as few as possible, at a time in the smallest supercell possible, while BID exploits perturbative derivatives for some order less than $\mathcal{N}$ (e.g., Hellman-Feynman forces) in order to extract all ID in the smallest possible supercells using the fewest possible computations. Finally, we derive an equation for the order N volume derivatives of the phonons in terms of the order $\mathcal{N} = N + 2$ ID. Given that the former are easily computed, they can be used as a stringent, infinite ranged test of the ID. Our general framework is illustrated on graphene, yielding irreducible phonon interactions to fifth order. Additionally, we provide a cost analysis for the rocksalt structure at $\mathcal{N} = 3$, demonstrating a massive speedup compared to popular finite displacement methods in the literature.

I. INTRODUCTION

A. General background

Phonons and phonon interactions dictate a wide array of materials properties, often including thermal conductivity, thermal expansion, linear and nonlinear elasticity, structural phase stability, and many other properties [1–5]. Even when studying purely electronic phenomena, knowledge of phonons and their interactions can be critical to interpreting experimental measurements. While computing phonons from first principles is largely considered a solved problem, practical shortcomings of existing methods still preclude their use on a broad swath of materials with select first-principles approaches. Furthermore, computing phonon interactions from first principles is still a rapidly evolving field, and the basic form of phonon interactions is not well known even in classic materials systems.

The problem of computing phonons and their interactions from first principles is equivalent to computing the Taylor series expansion of the Born-Oppenheimer energy surface with respect to the nuclear displacements of the crystal. The second-order terms (i.e., harmonic) dictate the phonons, while

higher-order terms (i.e., anharmonic) dictate phonon interactions. Given that a crystal is infinite in extent, the computed Taylor series at each order will necessarily be truncated at some maximum resolution. An important task is to obtain a sufficiently high resolution such that the expansion is converged at a given order, meaning that a higher resolution will have no appreciable influence on relevant observables.

There are two basic approaches to computing phonons [6,7] and the same can be claimed regarding their interactions: perturbation theory and finite displacements; where the latter encompasses usual finite difference approaches or more complicated fitting procedures based on finite displacements. Furthermore, these approaches are naturally combined, using perturbation theory to obtain some low-order derivatives (e.g., Hellman-Feynman forces) and finite displacements for higher-order derivatives. For an early example at second order within density functional theory (DFT), Ihm *et al.* used the Hellman-Feynman forces and finite difference to compute phonons [8]. In this same spirit, Bonini *et al.* used density functional perturbation theory (DFPT) to compute second-order terms and then used finite difference to compute third- and fourth-order terms in graphene [9].

In any case, whether it be perturbation theory or finite displacement or a combination thereof, the *de facto* standard is to compute all derivatives associated with displacements that transform as irreducible representations of some finite translation group (FTG) (i.e., q points commensurate with a Born-von-Karman supercell, described further in Sec. II B).

---

*lyuwen.fu@columbia.edu
†mckornbluth@gmail.com
‡chengzhengqian@gmail.com
§chris.marianetti@columbia.edu

This set of derivatives allows for a Fourier interpolation, which exactly preserves the derivatives at a q point that is an irreducible representation of the FTG while providing a smooth interpolation for all other q points (see Refs. [10,11] for early examples at second order). Assuming that the discretization errors of finite difference calculations are properly extrapolated to zero; and that spurious behavior is properly handled when encountered via perturbation theory (e.g., see Ref, [12]); and that the underlying first-principles approach is properly converged with respect to its own discretizations (e.g., plane wave cutoff, k-point density, etc); and that the energy function is analytic; then all approaches must agree on derivatives with respect to displacements which transform as irreducible representations of the FTG.

Within DFT at second order, it should be noted that a distinct advantage of perturbation theory (i.e., density functional perturbation theory) is that an arbitrary point within the Brillouin zone may be computed with a cost on the order of a standard DFT calculation of the primitive unit cell [7], while finite displacement approaches are limited to supercells for which a DFT calculation can be tractably performed. However, not all mainstream DFT codes have fully implemented DFPT yet. Moreover, perturbation theory is not ubiquitous for techniques which go beyond DFT, and even simple approaches like DFT $+ U$ only have a few demonstrations to date where perturbation theory has been executed at second order [13,14]. Therefore both perturbation theory and finite displacement approaches will continue to play an important role for the foreseeable future in the context of computing phonons and their interactions.

This paper describes several novel approaches, applicable to a broad variety of phonon and phonon-interaction methodologies. First, we write the Taylor series purely in terms of space group irreducible derivatives, building in all possible symmetry by construction; we are not aware of existing studies that employ this in complex scenarios beyond second order (i.e., for a sufficiently large FTG to describe generic observables). Aside from computational efficiency, symmetry is essential for characterizing, storing, and disseminating the vibrational Hamiltonian. Second, we devise two finite displacement approaches, which focus on getting the most precise answer or getting a robust answer as efficiently as allowed by group theory. Finally, we evaluate various approaches to assessing the integrity of the Taylor series.

The remainder of the paper is organized as follows. Sections I B–I E review the relevant literature with respect to group theory, perturbation theory, and previous approaches using finite displacements. Section II outlines our group theoretical methodology, which is illustrated throughout with examples from graphene for the sake of clarity. Additionally, a glossary of all key variables can be found in Ref. [15], Table SI. Section III puts forward our finite displacement approaches. Section III B solves the minimum supercell problem using the Smith normal form, resulting in the minimum supercell multiplicity equation; while Secs. III D–III F introduce our LID and BID finite displacement approaches. Finally, Sec. IV focusses on how to assess the quality of the extracted irreducible derivatives, including the Nth-order strain derivatives of the phonons.

Applications are presented throughout the manuscript, and DFT calculations were executed as follows (unless otherwise noted). DFT calculations within the local density approximation (LDA) [16] were performed using the projector augmented wave (PAW) method [17,18], as implemented in the Vienna *ab initio* simulation package (VASP) [19–22]. A plane wave basis with a kinetic energy cutoff of 625 eV was employed. We used a Γ-centered k-point mesh of $100 \times 100 \times 1$. All k-point integrations were done using Gaussian smearing with a smearing width of 0.2 eV. The DFT energies were converged to within 10^{-8} eV, while ionic relaxations were converged to within 10^{-7} eV. The relaxed lattice parameter in graphene was found to be $a_0 = 2.44994$ Å.

B. Symmetry and irreducible derivatives

Group theory is a central tenet of physics [23,24], and it should characterize phonons and their interactions; regardless of how these quantities are computed (i.e., finite displacement or perturbation theory). In the context of atomic physics, for example, where continuous groups characterize the invariance of the Hamiltonian, the notion of a "reduced matrix element" as given by the Wigner-Eckart theorem is textbook material [25]; and the same could be said for nuclear physics [26]. The beauty of reduced matrix elements is that absolutely no excess information needs to be provided, beyond the chosen phase conventions, to characterize any possible matrix element; and one is guaranteed that the theory satisfies symmetry by construction. Generically, we refer to this type of symmetrization as "intrinsic symmetrization," because it begins with basis functions that transform like irreducible representations of the group, and determines the existence of an arbitrary matrix element *a priori*.

In the context of lattice vibrations, the corresponding quantities are "space group irreducible derivatives" of the Born-Oppenheimer potential. Such an approach will automatically satisfy all space group symmetry by construction, in addition to homogeneity of free space and permutation symmetry of each derivative. At second order, space group irreducible derivatives are constructed using standard tools of solid state physics [23,27]: the irreducible Brillouin zone and the little group of a given q point. Beyond second order, the use of space group irreducible derivatives is far less common, most likely because the group theory is more complex. Nonetheless, constructing the symmetric products of irreducible representations of space groups was essentially a solved problem by the year 1980, and the history of this saga is well described by Cracknell *et al.* (see Vol. 1 of Ref. [28]). There are two complimentary approaches [29–36]: the full group approach and the subgroup approach. While both approaches have their respective merits, Cracknell *et al.* used the subgroup formulation of Gard [34,35] to completely automate the process, resulting in a code which could be executed at an arbitrary order $\mathcal{N}$ [28]; only limited by the computers of their time period. They produced printouts containing the selection rules for third-order symmetric products within all crystallographic space groups, and therefore the composition of the third-order Taylor series in terms of space group irreducible derivatives can be obtained for any possible crystal. They also report that they produced an archived volume with quartic symmetric products for all space groups.

Despite the power of intrinsic symmetrization in the context of lattice dynamics, which works with basis functions that transform as irreducible representations of the space group and obey clear selection rules which can be determined once and for all *a priori*, it remains highly underutilized; with applications beyond second order often involving Landau expansions, where a phase transition may be associated with a single star of wave vectors [37]; or optical transitions [36]. However, we are not aware of any systematic approach which utilizes intrinsic symmetrization to construct phonon interactions in general, which is an intent of this paper.

The major alternative to utilizing intrinsic symmetrization is to start with the order $\mathcal{N}$ Taylor series in real space (i.e., with displacements labeled by a lattice translation) and then impose invariance with respect to the space group operations, permutation symmetry of the derivative, and homogeneity and isotropy of free space [38–40]; and this results in a system of linear equations that the real-space derivatives must obey. This approach is the *direct opposite* of intrinsic symmetrization: instead of starting with symmetry and only creating allowed polynomials, one starts with the most general polynomials and then determines their relations. We refer to this alternate procedure as "extrinsic symmetrization." While extrinsic symmetrization is most naturally associated with a real-space basis, we note that it can be used for an arbitrary basis. Extrinsic symmetrization can be straightforwardly implemented in scenarios that are sufficiently low order and short range, allowing one to solve for a set of irreducible real-space derivatives. However, this approach quickly becomes challenging as the size of the initial unsymmetrized polynomial will grow rapidly with order and range.

Practitioners typically numerically implement extrinsic symmetrization while simultaneously fitting the real-space derivatives, resulting in a procedure where it is unclear to the outside observer if symmetry is actually being fulfilled. This even happens regularly at second order. For example, in the well known paper of Parlinski *et al.*, which puts forward an approach to compute phonons using finite difference [11], they implement point symmetry using extrinsic symmetrization and apply this to the case of ZrO_2. For a $2 \times 2 \times 2$ supercell relative to the conventional cubic cell, their symmetry analysis finds that there are 68 independent parameters, though they report that only 59 of these 68 are nonzero. Nonetheless, group theory dictates that there are precisely 52 irreducible derivatives, all of which can be chosen as real numbers (see Appendix B for details). Strictly speaking, their Born-Oppenheimer potential will not satisfy symmetry, though their results are clearly robust and not affected by this inefficacy. However, it is also worth noting that group theory dictates that all irreducible derivatives can be extracted with a single central finite difference measurement instead of two which are used in their study (see Secs. III C and III E for background and Appendix B for detailed results). Clearly, it is much easier to employ intrinsic symmetrization instead of a numerical implementation of extrinsic symmetrization where the answer is not obvious. While the aforementioned paper is relatively old, extrinsic symmetrization still persists at second order [41–43] and is commonplace beyond second order [44–47]. More importantly, we demonstrate that the practical inefficacy of extrinsic symmetrization is dramatically worse

in some popular approaches for computing cubic interactions (see Sec. III E).

An important point to consider is how the Taylor series is truncated at a given order, and there are two natural approaches to doing this. First, one can create a homomorphic mapping between the infinite translation group and a finite translation group (FTG) via a Born von Karman (BvK) supercell [23,27]; and this type of truncation is naturally compatible with the irreducible representations of the space group and the accompanying intrinsic symmetrization. Second, one can retain the infinite crystal, or a sufficiently large BvK supercell, and define a range in real-space via nearest neighbor shells or some cluster size beyond which all derivatives are zero; and this type of truncation is naturally compatible with a real-space basis and extrinsic symmetrization. We refer to these two types of truncation as reciprocal space truncation and real-space truncation, respectively, given that the former restricts to some finite number of q points and the latter restricts to some neighbor shell in real space. An important point to realize is that these two truncations do not have a direct correspondence in general, and it is often not clear which truncation a practitioner is using.

An additional important point is that translation group irreducible derivatives, and therefore space group irreducible derivatives as well, *are invariant to the supercell in which they are computed*, whereas real-space derivatives are only exact in the infinite crystal. Of course, a real-space basis can always be used in any supercell, even very small supercells, but in such situations the real-space derivatives are simply containers and interpolants for the space group irreducible derivatives. Under normal circumstances, the real-space derivatives will converge when taken in a sufficiently large supercell, but space group irreducible derivatives are always converged with respect to supercell size by construction. However, a sufficient number of space group irreducible derivatives must be resolved in order to precisely interpolate to an arbitrary q point, which is equivalent to the real-space derivatives being sufficiently diminished within the truncation range.

Finally, we point out that there is a middle ground between intrinsic and extrinsic symmetrization, which can be convenient if a real-space truncation is needed. One can consider the crystal to be an infinite array of overlapping clusters, and the local modes of each cluster can then be used as the new degrees of freedom subject to a constraint. Such a program was originally put forth and implemented for model Hamiltonians in two dimensions [48–50]. The same type of framework, called the slave mode expansion, was put forward purely for the purpose of symmetrizing the lattice potential [51,52]. The basic idea is to perform intrinsic symmetrization with respect to the point group, and then to perform extrinsic symmetrization with respect to the translation group; assuming that the clusters overlap (see Ref. [53] for an approach similar in spirit, yet distinct).

C. Perturbation theory

Perturbation theory is normally the preferred method for computing derivatives, and should be used when possible. The Hellman-Feynman theorem provides first derivatives of the energy (i.e., the force) at a very small computational cost [6],

and have become standard in density functional theory codes. Perturbative forces are often implemented in static approaches like DFT $+ U$, and a few studies have succeeded in computing forces in more advanced methods such as DFT plus dynamical mean-field theory [54,55].

For second-order derivatives, density functional perturbation theory (DFPT) [7,56–59] may be executed at an arbitrary reciprocal space point, with a cost which is on the order of a primitive cell self-consistent DFT calculation [7]; and there is a large literature of such calculations. DFPT is not as widely available as the ubiquitous Hellman-Feynman forces, and therefore DFPT may not be available for all codes or basis sets in practice. Furthermore, DFPT often does not support even simple beyond DFT methods such as DFT $+ U$, and at present we are only aware of several examples in the literature [13,14]. Therefore DFPT is not always an option for second-order derivatives.

DFPT may be extended to third order [58–60], and this has been implemented for the most general case (i.e. arbitrary q vectors, metals and insulators) [61,62]. A small number of applications can be found in the literature thus far [63–68]. We are not aware of any studies using third-order DFPT within DFT $+ U$.

DFPT naturally works with irreducible derivatives of the translation group, and at least some implementations at second order work with irreducible representations of the space group when performing perturbation theory [69]. It is unclear to what extent point symmetry, or full space group symmetry, is exploited for third order. In any case, it would be ideal if DFPT studies reported space group irreducible derivatives, as this would allow for a direct comparison with competing methods.

D. Finite displacement phonon approaches

Finite displacement approaches are those which explicitly move the atoms in a series of different displacement fields and perform a full, self-consistent first-principles calculation in each case. This could range from performing a first-principles molecular dynamics trajectory, to a more standard central or forward finite difference calculation; and we focus on the latter. We begin by reviewing the earliest papers in the literature, and discuss them in terms of the framework we will be presenting. Perhaps the earliest study performed second and third-order finite difference derivatives of the energy using a displacement which transforms as an irreducible representation of the space group [70], and this came to be known as a "frozen-phonon" calculation. In terms of our categorization, the preceding paper falls under LID with PD_0 (see Sec. III D).

Several similar studies followed soon after on various materials [8,71,72], and Ihm *et al.* used the Hellman-Feynman forces in this same context [8], which we categorize as LID using PD_1. Martin subsequently announced a major advance which further exploited Hellman-Feynman forces [73], whereby the displacement field was intentionally chosen not to transform as an irreducible representation of the space group such that many independent force constants could be simultaneously measured. This general philosophy falls under the category of second-order SS-BID (see Sec. III E). A subsequent study then executed Martin's previous announcement with an application to GaAs [74], showing the power of

this approach. However, several additional steps would be needed to satisfy all the conditions of SS-BID. First, the force constants should be extracted in a manner which preserves the irreducible derivatives of the translation group. Second, the approach for displacing the atoms could be optimized.

In order to better exploit the forces, displacement should be constructed so as to sample as many irreducible derivatives as possible in a single calculation. Frank *et al.* made another step forward, performing finite difference calculations where they displaced a single atom at a time [75]. This approach goes a long way towards achieving the goal, given that a local displacement in real space is guaranteed to sample all q points in the supercell; though a shortcoming is that point symmetry is not explicitly dealt with in any way. More problematic is that care is needed to ensure the translation group irreducible derivatives are extracted properly.

Parlinski *et al.* resolved a main shortcoming of the preceding studies [11], introducing a proper weighting of the real-space force constants on the boundary of the Wigner-Seitz supercell, which ensures their Fourier interpolation yields the numerically exact irreducible derivatives of the finite translation group for the supercell being used. The authors also directly account for point symmetry, determining the minimum number of calculations required to extract all force constant in conjunction with the forces (though there were some inefficacies in their analysis, see discussion in Sec. I B). We categorize this method as a second-order SS-BID approach (see Sec. III E). The same categorization would be applied to the similar algorithms used in the software packages PHONOPY [43] and PHON [41].

A relevant factor which had not been considered by the aforementioned approaches is that they extract all force constants from a single supercell, and we refer to these as *single supercell* (SS) approaches. An important development occurred relatively recently with the work of Monserrat *et al.* [76], which recognized the importance of using so-called nondiagonal supercells. They show that given a three dimensional crystal, all q points within a $n_1 \times n_2 \times n_3$ supercell can always be probed in supercells containing lcm (n_1, n_2, n_3) primitive cells. This result has far reaching implications for computing phonons, offering a massive speedup for first-principles approaches which scale in a superlinear manner. It should be noted that their result is a special case of our minimum supercell multiplicity equation (36), and Eq. (37) which follows. We categorize their method as a hierarchical supercell approach, similar to HS-BID for the specific case of $\mathcal{N} = 2$. We emphasize that single supercell approaches offer absolutely no extra information (i.e., irreducible derivatives) as compared to hierarchical supercell approaches.

E. Finite displacement anharmonic approaches

Finite displacement approaches have also been employed to compute anharmonic terms. As mentioned, the very first frozen phonon calculation by Wendel and Martin computed a third-order derivative using finite difference of the energy [70]. More systematic approaches began to appear thereafter, such as when Vanderbilt *et al.* used the forces and finite displacement calculations to fit an assortment of cubic and quartic phonon interactions at products of the Γ and X points

in diamond [77,78]. These interactions were then fit to a modified Keating model which was then used to extrapolate throughout the Brillouin zone; and this approach provided reasonable results for the phonon lifetimes in Si.

As time progressed and computing resources increased, new efforts emerged to systematically compute more interactions. Esfarjani and Stokes employed an extrinsic symmetrization approach with a real-space truncation (see Sec. I B) in order to compute the real-space force constants up to fourth order [44]. They suggested that a data set of forces could be obtained from DFT calculations on a sufficiently large supercell by generating a first-principles molecular dynamics trajectory, random displacements, or symmetrically displacing one atom at a time; and they opted for the latter in a test on Si. Using this data set and the aforementioned symmetrization constraints, they fit the real-space force constants up to fourth order. Applications of this method in a wide range of materials soon followed, all in the context of thermal conductivity [79–82]. Many approaches similar to the aforementioned approach, yet distinct in various ways, soon followed [45,47,51,53,83–85], with each producing the real-space force constants up to some order and within some real-space truncation range. In Sec. III E, we compare our SS-BID approach to several of the aforementioned approaches [45,84,85], demonstrating that we can extract all space group irreducible derivatives far more efficiently for a given test case in rock salt. Furthermore, all of the above approaches could benefit from our hierarchical supercell approach (see Secs. III B and III F).

While all the preceding studies relied upon forces (i.e., PD_1), third and fourth-order phonon interactions have been computed using finite difference of second-order DFPT calculations in graphene and graphite [9]. In that study, a FTG is used for truncation (i.e., with graphene, they used $\hat{\mathbf{S}}_{BZ} = 4\hat{\mathbf{I}}$ for $\mathcal{N} = 3$ and $\mathcal{N} = 4$ with PD_2) instead of a real-space truncation, and the cubic and quartic derivatives appear to be translation group irreducible. A study of this sort could fully exploit both the SS-BID and the HS-BID approaches we outline in this paper, which would yield a major increase in efficiency (see Secs. III E and III F).

II. GROUP THEORETICAL METHODOLOGY

A. Crystalline potential and its derivatives

We begin by discussing the Born-Oppenheimer potential energy, V, defined over the set of all nuclear displacements in the crystal, $\{u_{\mathbf{t}}^{(b,\beta)}\}$; where $\mathbf{t}$ labels a unit cell in lattice coordinates, b labels one of the n_a different atoms within the unit cell, and β labels one of the n_p possible displacements of the atom. The function V is invariant to all operations of some space group and conserves total linear and angular momentum; and V is presumed to be analytic. Our convention is to define V as the energy of the crystal *per unit cell*, so it is an intensive quantity. While we focus on V in this work, any function defined over the lattice could be considered. Due to the large number of variables defined in this paper, a glossary is provided in Ref. [15], Table SI. Additionally, our application to graphene is distributed throughout the manuscript, which should aid in understanding all definitions.
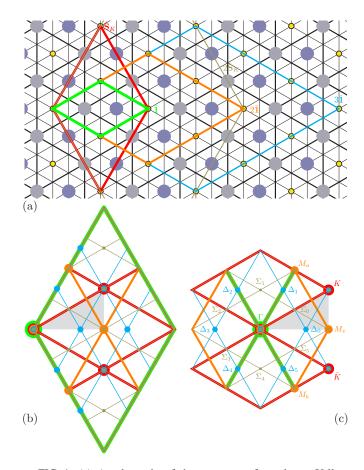

FIG. 1. (a) A schematic of the structure of graphene. Yellow hexagons are lattice points, while circles represent carbon atoms. The first five smallest BvK supercells are pictured, and the lattice points of a corresponding FTG is given by Eq. (7). (b) The corresponding (color coded) five reciprocal lattice subcells which are repeated to tile the first Brillouin zone (FBZ); irreducible Brillouin zone is shaded grey. (c) Same as (b), but with the FBZ in the Wigner-Seitz cell convention. All q-points are labeled according to their star.

If the crystal is d-dimensional, the translation group is defined via d linearly independent vectors $\mathbf{a}_i$ in $\mathbb{R}^d$, and stored as row-stacked vectors in the rank-d matrix $\hat{\mathbf{a}}$ (matrices are always denoted with a hat). An arbitrary lattice point may be expressed as $\mathbf{t}\hat{\mathbf{a}}$, where $\mathbf{t}$ is a d-dimensional row vector of integers: $\mathbf{t} \in \mathbb{Z}^d$. Basis atoms are specified as n_a distinct Cartesian vectors $\mathbf{A}_i$. A corresponding set of reciprocal lattice vectors are defined as $\hat{\mathbf{b}} = 2\pi(\hat{\mathbf{a}}^{-1})^{\mathsf{T}}$, where $\hat{\mathbf{b}}$ gives the row stacked vectors $\mathbf{b}_i$. An arbitrary point in reciprocal space may be expressed as $\mathbf{q}\hat{\mathbf{b}}$, where $\mathbf{q}$ is a d-dimensional row vector of real numbers: $\mathbf{q} \in \mathbb{R}^d$. The continuum of q points within the first Brillouin zone can be used to form basis functions $\{u_{\mathbf{q}}^{(b,\beta)}\}$ that transform like irreducible representations of the translation group. For the case of graphene [see schematic in Fig. 1(a)], we have

$$\hat{\mathbf{a}} = \frac{a_0}{2}\begin{bmatrix} \sqrt{3} & 1 \\ \sqrt{3} & -1 \end{bmatrix}, \quad \hat{\mathbf{b}} = \frac{2\pi}{a_0\sqrt{3}}\begin{bmatrix} 1 & \sqrt{3} \\ 1 & -\sqrt{3} \end{bmatrix}, \quad (1)$$

$$\mathbf{A}_1 = a_0\frac{\sqrt{3}}{3}\mathbf{i}, \quad \mathbf{A}_2 = a_0\frac{2\sqrt{3}}{3}\mathbf{i}, \quad (2)$$

where $a_0 = 2.44994$ Å, as computed within DFT (see Sec. I A for computational details), and **i** is the unit vector for the horizontal axis.

An $\mathcal{N}$th-order derivative of V is denoted as $V_{i_1...i_{\mathcal{N}}}^{j_1...j_{\mathcal{N}}}$, where i labels either some linear combination of reciprocal lattice vectors or real lattice vectors, and j labels some linear combination of the $n_a n_p$ degrees of freedom within the unit cell. For the specific case of derivatives taken with respect to the displacements in the real lattice basis, we define the force tensor

$$\Phi_{\mathbf{0}\ \ \mathbf{t}_2-\mathbf{t}_1\ ...\mathbf{t}_{\mathcal{N}}-\mathbf{t}_1}^{(b_1,\beta_1)(b_2,\beta_2)...(b_{\mathcal{N}},\beta_{\mathcal{N}})} = \frac{\partial^{\mathcal{N}}V}{\prod_i^{\mathcal{N}}\partial u_{\mathbf{t}_i-\mathbf{t}_1}^{(b_i\beta)}}, \tag{3}$$

where we explicitly retain the identity translation **0** as the first index (i.e., $\mathbf{t}_1 - \mathbf{t}_1 = \mathbf{0}$), and $u_{\mathbf{t}_i}^{(b_i,\beta_i)}$ follows the same convention as previously defined. For the specific case of derivatives taken with respect to displacements that transform as irreducible representations of the translation group, we define the dynamical tensor:

$$D_{\mathbf{q}_1\ \ ...\mathbf{q}_{\mathcal{N}}}^{(b_1,\beta_1)...(b_{\mathcal{N}},\beta_{\mathcal{N}})} = \frac{\partial^{\mathcal{N}}V}{\prod_i^{\mathcal{N}}\partial u_{\mathbf{q}_i}^{(b_i,\beta_i)}}, \tag{4}$$

where $\sum_{i=1}^{\mathcal{N}} \mathbf{q}_i \in \mathbb{Z}^d$ and b_i, β_i follows the same convention as previously defined.

B. Finite translation group

Here we define the familiar notion of the finite translation group (FTG), which is a homomorphic mapping with the infinite translation group via periodic boundary conditions [23,27]; though we consider the most general case. The FTG is equivalently defined using a supercell of the real space lattice or a subcell of the reciprocal lattice; which we refer to as the Born-von Karman (BvK) supercell and Brillouin zone (BZ) subcell, respectively. We note that nondiagonal BvK supercells are considered in this work. Mathematically, we define the BvK supercell lattice vectors of the real-space lattice and the corresponding BZ subcell vectors of the reciprocal lattice using the matrix $\hat{\mathbf{S}}_{\text{BZ}}$:

$$\hat{\mathbf{a}}_{\text{BZ}} = \hat{\mathbf{S}}_{\text{BZ}}\hat{\mathbf{a}}, \quad \hat{\mathbf{b}}_{\text{BZ}} = (\hat{\mathbf{S}}_{\text{BZ}}^{-1})^{\mathsf{T}}\hat{\mathbf{b}}, \tag{5}$$

where

$$\hat{\mathbf{S}}_{\text{BZ}} \in \{\hat{\mathbf{n}} \in \mathbb{Z}^{(d,d)} : \det(\hat{\mathbf{n}}) \neq 0,$$

$$\hat{\mathbf{n}}\hat{\mathbf{a}}\hat{\mathbf{R}}^{\mathsf{T}}(\hat{\mathbf{n}}\hat{\mathbf{a}})^{-1} \in \mathbb{Z}^{(d,d)}\forall\hat{\mathbf{R}} \in \tilde{G}\}, \tag{6}$$

where d is the dimension of the crystal and $\tilde{G}$ is the point group of the space group (sets are always denoted with a tilde). In words, $\hat{\mathbf{S}}_{\text{BZ}}$ is an invertible $d \times d$ matrix of integers, with a real (reciprocal) space Wigner-Seitz super (sub) cell that is invariant to $\tilde{G}$.

The translation vectors of the FTG are all integer combinations of rows of $\hat{\mathbf{a}}$ that fit within the d-dimensional parallelotope formed from the rows of $\hat{\mathbf{a}}_{\text{BZ}}$, while the corresponding reciprocal lattice points are given by all integer combinations of rows of $\hat{\mathbf{b}}_{\text{BZ}}$ that fit within the d-dimensional parallelotope formed from the rows of $\hat{\mathbf{b}}$. Mathematically, a translation vector of the FTG is represented as $\mathbf{t}\hat{\mathbf{a}}$, where $\mathbf{t}$ is a row vector of integers $\mathbf{t} \in \mathbb{Z}^d$ constrained to

$$0 \leqslant \mathbf{t}\hat{\mathbf{S}}_{\text{BZ}}^{-1} \cdot \mathbf{e}_j < 1 \quad \text{for} \quad j = 1,\ldots,d, \tag{7}$$

where $\mathbf{e}_j$ is a unit vector in $\mathbb{Z}^d$. We refer to $\mathbf{t}$ as a "t point" and the set of all $\mathbf{t}$ satisfying Eq. (7) is defined as $\tilde{t}_{\text{BZ}}$. Similarly, a reciprocal lattice point is represented as $\mathbf{p}\hat{\mathbf{b}}_{\text{BZ}}$, where $\mathbf{p}$ is a row vector of integers $\mathbf{p} \in \mathbb{Z}^d$ constrained to

$$0 \leqslant \mathbf{p}(\hat{\mathbf{S}}_{\text{BZ}}^{-1})^{\mathsf{T}} \cdot \mathbf{e}_j < 1 \quad \text{for} \quad j = 1,\ldots,d. \tag{8}$$

When a reciprocal lattice point $\mathbf{p}\hat{\mathbf{b}}_{\text{BZ}}$ is denoted in lattice coordinates of $\hat{\mathbf{b}}$, it will be a vector of fractions less than one: $\mathbf{q} = \mathbf{p}(\hat{\mathbf{S}}_{\text{BZ}}^{-1})^{\mathsf{T}}$. We naturally refer to $\mathbf{q}$ as a "q point." The set of all $\mathbf{q}$ obtained from all $\mathbf{p}$ satisfying Eq. (8) is denoted as $\tilde{q}_{\text{BZ}}$, which is a discretization of the first Brillouin zone. The characters of the irreducible representations of the FTG are then $e^{i2\pi\mathbf{t}\cdot\mathbf{q}}$. It should be appreciated that all q points are identity representations of the supercell translation group given that $\mathbf{q}\hat{\mathbf{S}}_{\text{BZ}}^{\mathsf{T}} \in \mathbb{Z}^d$, and therefore all waves corresponding to q points are commensurate with $\hat{\mathbf{S}}_{\text{BZ}}$.

Given the importance of the total number of t points (or q points), we define the variable $n_q = |\tilde{t}_{\text{BZ}}| = |\tilde{q}_{\text{BZ}}| = |\det(\hat{\mathbf{S}}_{\text{BZ}})|$, and this number also characterizes the *supercell multiplicity*, which is the number of primitive cells contained within the supercell. An efficient algorithm for determining $\tilde{t}_{\text{BZ}}$ and $\tilde{q}_{\text{BZ}}$, which requires solving Eqs. (7) and (8), is given in Appendix D. If the column and row Hermite normal form [86] of $\hat{\mathbf{S}}_{\text{BZ}}$ are identical under transpose, the set of allowed $\mathbf{t}$ is identical to the set of allowed $\mathbf{p}$; which is a typical scenario. Another key property of the FTG is the least common denominator of all components of all $\mathbf{q} \in \tilde{q}_{\text{BZ}}$, denoted L_m. In the common case of $\hat{\mathbf{S}}_{\text{BZ}} = n\hat{\mathbf{1}}$, where $n \in \mathbb{Z}_+$ and $\hat{\mathbf{1}}$ is the rank-d identity matrix, we simply have $L_m = n$; and we refer to this as a *uniform* supercell.

The symmetrized displacement amplitudes are obtained with the projection operator, recovering the usual discrete Fourier transform, though we use a normalization such that the q-space amplitudes are intensive quantities:

$$u_{\mathbf{q}}^{(b,\beta)} = \frac{1}{n_q}\sum_{\mathbf{t}\in\tilde{t}_{\text{BZ}}}u_{\mathbf{t}}^{(b,\beta)}e^{-2\pi i\mathbf{t}\cdot\mathbf{q}}, \tag{9}$$

$$u_{\mathbf{t}}^{(b,\beta)} = \sum_{\mathbf{q}\in\tilde{q}_{\text{BZ}}}u_{\mathbf{q}}^{(b,\beta)}e^{2\pi i\mathbf{t}\cdot\mathbf{q}}, \tag{10}$$

where these modes are imparted on some supercell $\hat{\mathbf{S}}_{\text{BZ}}$.

In the case of graphene, it is straightforward to find that all FTG can be obtained as integer multiples of the rank 2 identity matrix $\hat{\mathbf{1}}$ or the supercell $\hat{\mathbf{S}}_K = 2\hat{\mathbf{1}} - \hat{\sigma}_x$, where $\hat{\sigma}_x$ is a Pauli matrix; and this results in grid densities of $n_q = \{n^2|n \in \mathbb{Z}^+\}$ and $n_q = \{3n^2|n \in \mathbb{Z}^+\}$ points per Brillouin zone, respectively (see schematic in Figures 1(a-c) for FTG corresponding to $\hat{\mathbf{S}}_{\text{BZ}} = \hat{\mathbf{1}}$, $\hat{\mathbf{S}}_K$, $2\hat{\mathbf{1}}$, $3\hat{\mathbf{1}}$, and $2\hat{\mathbf{S}}_K$). While the FTG $\hat{\mathbf{1}}$ is already nontrivial given that $n_a > 1$ in graphene, it is pedagogically instructive to consider the next largest FTG with $\hat{\mathbf{S}}_{\text{BZ}} = \hat{\mathbf{S}}_K$; which corresponds to the order 3 cyclic group. For this FTG, $n_q = 3$ and we have

$$\tilde{t}_{\text{BZ}} = \{(0,0), (1,0), (0,1)\} = \{\mathbf{0}, \mathbf{t}_a, \mathbf{t}_b\}, \tag{11}$$

$$\tilde{q}_{\text{BZ}} = \left\{(0,0), \left(\frac{2}{3},\frac{1}{3}\right), \left(\frac{1}{3},\frac{2}{3}\right)\right\} = \{\Gamma, K, \bar{K}\}, \tag{12}$$

which can be deduced from the diagrams in Fig 1.

C. Point symmetry of finite translation group

The point symmetry of the FTG must also be considered, and several additional definitions are needed. First, $\tilde{t}_{IBZ}$ and $\tilde{q}_{IBZ}$ are irreducible sets which can generate all elements of $\tilde{t}_{BZ}$ and $\tilde{q}_{BZ}$, respectively, in conjunction with some point operation $\hat{\mathbf{R}} \in \tilde{G}$. Furthermore, it is important to identify the so-called "little group" $\tilde{G}_{\mathbf{q}}$ for each $\mathbf{q} \in \tilde{q}_{IBZ}$, which is the subgroup of $\tilde{G}$ that leaves $\mathbf{q}$ invariant to within a shift in $\mathbb{Z}^d$. Finally, we must introduce the "star" of the q point, which is the set of points generated by $\tilde{G}$: $\tilde{s}_{\mathbf{q}} = \{\mathbf{q}\hat{\mathbf{b}}\hat{\mathbf{R}}^\intercal\hat{\mathbf{b}}^{-1}|\forall\hat{\mathbf{R}} \in \tilde{G}\}$, where $|\tilde{s}_{\mathbf{q}}| \leqslant h$, and h is the order of the group $\tilde{G}$; and there will be one star for each $\mathbf{q} \in \tilde{q}_{IBZ}$. The set of all stars is then denoted as $\tilde{s}_{BZ} = \{\tilde{s}_{\mathbf{q}}|\forall\mathbf{q} \in \tilde{q}_{IBZ}\}$. A given star may be used to create a $|\tilde{s}_{\mathbf{q}}|$-dimensional representation of star vectors.

In the case of graphene, we have $\tilde{G} = D_{6h}$, using Schoenflies notation. For $\hat{\mathbf{S}}_{BZ} = \hat{\mathbf{S}}_K$, $\tilde{q}_{IBZ} = \{\Gamma, K\}$; the little groups are $\tilde{G}_\Gamma = D_{6h}$ and $\tilde{G}_K = D_{3h}$; the two stars are $\tilde{s}_\Gamma = \{\Gamma\}$ and $\tilde{s}_K = \{K, \bar{K}\}$, and the corresponding representations of the star vectors decompose to A_{1g} and $A_{1g} \oplus B_{2u}$, respectively.

D. Order $\mathcal{N}$ identity representations of FTG and permutation symmetry

Having defined the FTG, the resolution of the problem has been set. We proceed by creating all of the order $\mathcal{N}$ direct product representations of $\tilde{q}_{BZ}$ which transform like the identity under the translation group. Each identity representation is given by an $\mathcal{N}$-tuple denoted as $\mathcal{Q} = (\mathbf{q}_1, \dots, \mathbf{q}_\mathcal{N})$, and this quantity will also be needed as a row stacked matrix, denoted $\hat{\mathcal{Q}}$. The translation group demands that the identity representation satisfy $(\sum_{\mathbf{q} \in \mathcal{Q}} \mathbf{q}) \in \mathbb{Z}^d$. Clearly, one of the $\mathbf{q} \in \mathcal{Q}$ is not independent, and there must be $n_q^{\mathcal{N}-1}$ distinct identity representations. Therefore we can identify each order $\mathcal{N}$ identity irreducible representation with a corresponding element of the $\mathcal{N} - 1$ direct product group formed from $\tilde{t}_{BZ}$, denoted as the $\mathcal{N}$ tuple of vectors $\mathcal{T} = (\mathbf{0}, \mathbf{t}_1, \dots, \mathbf{t}_{\mathcal{N}-1})$; this quantity will also be needed as a row stacked matrix, denoted $\hat{\mathcal{T}}$. Within the BvK supercell, the set of all $\mathcal{T}$ is denoted $\tilde{\mathcal{T}}_{\hat{\mathbf{S}}_{BZ}}$, and the set of all identity representations $\mathcal{Q}$ is denoted as $\tilde{\mathcal{Q}}_{\hat{\mathbf{S}}_{BZ}}$ (abbreviated as $\tilde{\mathcal{T}}_{BZ}$ and $\tilde{\mathcal{Q}}_{BZ}$, respectively). For the case of graphene with $\mathcal{N} = 3$ and $\hat{\mathbf{S}}_{BZ} = \hat{\mathbf{S}}_K$, we have

$$\tilde{\mathcal{Q}}_{BZ} = \{(\Gamma, \Gamma, \Gamma), (\Gamma, \bar{K}, K), (\Gamma, K, \bar{K}), (K, \Gamma, \bar{K})$$
$$(\bar{K}, \Gamma, K), (K, \bar{K}, \Gamma), (\bar{K}, K, \Gamma), (K, K, K),$$
$$(\bar{K}, \bar{K}, \bar{K})\}$$
$$= \{\mathcal{Q}_1, \mathcal{Q}_2, \mathcal{Q}_3, \mathcal{Q}_4, \mathcal{Q}_5, \mathcal{Q}_6, \mathcal{Q}_7, \mathcal{Q}_8, \mathcal{Q}_9\}; \quad (13)$$
$$\tilde{\mathcal{Q}}_{IBZ} = \{(\Gamma, \Gamma, \Gamma), (\Gamma, \bar{K}, K), (K, \Gamma, \bar{K}), (K, \bar{K}, \Gamma),$$
$$(K, K, K)\}$$
$$= \{\mathcal{Q}_1, \mathcal{Q}_2, \mathcal{Q}_4, \mathcal{Q}_6, \mathcal{Q}_8\}; \quad (14)$$
$$\tilde{\mathcal{T}}_{BZ} = \{(\mathbf{0}, \mathbf{0}, \mathbf{0}), (\mathbf{0}, \mathbf{0}, \mathbf{t}_a), (\mathbf{0}, \mathbf{0}, \mathbf{t}_b), (\mathbf{0}, \mathbf{t}_a, \mathbf{0}), (\mathbf{0}, \mathbf{t}_a, \mathbf{t}_a),$$
$$(\mathbf{0}, \mathbf{t}_a, \mathbf{t}_b), (\mathbf{0}, \mathbf{t}_b, \mathbf{0}), (\mathbf{0}, \mathbf{t}_b, \mathbf{t}_a), (\mathbf{0}, \mathbf{t}_b, \mathbf{t}_b)\}. \quad (15)$$

Given that any derivative is invariant to permutation symmetry, it is necessary to define a *multiset* $Q = [\mathbf{q} \in \mathcal{Q}]$ (multisets augment sets to allow for repeated elements; no special

demarcation is given to the variable), where multisets are denoted with square brackets. We can immediately reduce $\tilde{Q}_{BZ}$ to the identity representations of the symmetric product group by retaining only the unique Q generated from $\tilde{\mathcal{Q}}_{BZ}$; and this is denoted $\tilde{Q}_{BZ}$. Finally, we can create the point irreducible set of $\tilde{Q}_{BZ}$, denoted as $\tilde{Q}_{IBZ}$. For the case of graphene with $\mathcal{N} = 3$ and $\hat{\mathbf{S}}_{BZ} = \hat{\mathbf{S}}_K$, we have

$$\tilde{Q}_{BZ} = \{[\Gamma, \Gamma, \Gamma], [\Gamma, \bar{K}, K], [K, K, K], [\bar{K}, \bar{K}, \bar{K}]\}$$
$$= \{Q_1, Q_2, Q_3, Q_4\}; \quad (16)$$
$$\tilde{Q}_{IBZ} = \{[\Gamma, \Gamma, \Gamma], [\Gamma, \bar{K}, K], [K, K, K]\}$$
$$= \{Q_1, Q_2, Q_3\}. \quad (17)$$

For each $Q \in \tilde{Q}_{IBZ}$, all distinct Q_i that are generated from point operations form a star, denoted as $\tilde{\mathcal{S}}_Q$ (where $1 \leqslant |\tilde{\mathcal{S}}| \leqslant h$).

$$\tilde{\mathcal{S}}_{Q_1} = \{Q_1\}, \quad \tilde{\mathcal{S}}_{Q_2} = \{Q_2\}, \quad \tilde{\mathcal{S}}_{Q_3} = \{Q_3, Q_4\}. \quad (18)$$

The set composed of all such stars is denoted $\tilde{\mathcal{S}}_{BZ}$ (where $|\tilde{\mathcal{S}}_{BZ}| = |\tilde{Q}_{IBZ}|$).

Finally, it will be useful to define a sorting operator $\mathbb{S}$, based on a chosen convention, to generate a particular $\mathcal{Q}$ from a given Q [e.g., $\mathbb{S}([\Gamma, \bar{K}, K]) = (\Gamma, \bar{K}, K)$]. The illustrated convention corresponds to sorting the vectors according to their lattice coordinates within the conventional FBZ [i.e., coordinates from Fig. 1(b)].

E. Point symmetry including the basis

Having accounted for translation, permutation, and point symmetry of the order $\mathcal{N}$ identity representations of the pure lattice, point symmetry of the atoms and their corresponding displacements vectors must now be incorporated. First, one must symmetrize the $n_a n_p$ displacements $\{u_{\mathbf{q}}^{(b,\beta)}\}$ for all $\mathbf{q} \in \tilde{q}_{IBZ}$ according the little group of each respective $\mathbf{q}$, resulting in a set of symmetrized displacements $\{u_{\mathbf{q}}^{(\alpha,a)}\}$, where α labels a given irreducible representation and a labels a corresponding row of α. The resulting irreducible representation labels of the displacements at a given $\mathbf{q}$ are stored in the multiset $\mathcal{U}_{\mathbf{q}}$, and $\hat{\mathcal{U}}_{\mathbf{q}}$ will denote the direct sum of the irreducible representation matrices. For the case of $\mathbf{q} = M_x$ [see Fig. 1(c)], for example, we have displacements that transform as the following six irreducible representations:

$$\mathcal{U}_{M_x} = \{A_{1g}, B_{2g}, B_{3g}, B_{1u}, B_{2u}, B_{3u}\}. \quad (19)$$

We tabulate the explicit form of all symmetrized displacements of graphene, for all $\mathbf{q} \in \tilde{q}_{BZ}$, in Ref. [15], Table SII. All point group conventions in this study follow Cornwell [23].

Given some $Q \in \tilde{Q}_{IBZ}$ at order $\mathcal{N}$, where $Q = [\mathbf{q}_1 \dots \mathbf{q}_\mathcal{N}]$, the task at hand is to determine if a given derivative with respect to $u_{\mathbf{q}_1}^{(\alpha_1,a_1)} \dots u_{\mathbf{q}_\mathcal{N}}^{(\alpha_\mathcal{N},a_\mathcal{N})}$, where a_i denotes a row of an irreducible representation α_i of the little group of $\mathbf{q}_i$, is symmetry allowed; and if so, to determine how many irreducible derivatives it yields (in the case where multidimensional irreducible representations are present). Each displacement $u_{\mathbf{q}_i}^{(\alpha_i a_i)}$ will be associated with a set of star displacement vectors $\{u_{\tilde{\mathcal{S}}_{\mathbf{q}_i}}^{(\alpha',a')}\}$ of length $|\tilde{s}_{\mathbf{q}_i}|$, which form full space group irreducible representations [29]. Therefore the existence of derivatives with

TABLE I. A table of the irreducible derivatives for graphene at $\mathcal{N} = 2$ and $\mathcal{N} = 3$ with $\hat{S}_{BZ} = \hat{S}_K$. Units are eV/ $\mathring{A}^{\mathcal{N}}$.

Derivative	Value	Derivative	Value
$d_{\Gamma \ \ \Gamma}^{B_{2g}B_{2g}}$	35.417	$d_{\Gamma \ \ \Gamma}^{E_{2g}E_{2g}}$	113.986
$d_{\bar{K} \ \ K}^{A_1'A_1'}$	80.806	$d_{\bar{K} \ \ K}^{A_2'A_2'}$	43.951
$d_{\bar{K} \ \ K}^{E'E'}$	69.174	$d_{\bar{K} \ \ K}^{E''E''}$	12.708
$d_{\Gamma \ \ \Gamma \ \ \Gamma}^{E_{2g}E_{2g}E_{2g}}$	425.751	$d_{K \ \ K \ \ K}^{A_1'A_1'A_1'}$	440.064
$d_{K \ \ K \ \ K}^{A_1'A_2'A_2'}$	11.138	$d_{K \ \ K \ \ K}^{A_1'E'E'}$	289.379
$d_{K \ \ K \ \ K}^{A_1'E''E''}$	−53.543	$d_{K \ \ K \ \ K}^{E'E'E'}$	−239.640
$d_{K \ \ K \ \ K}^{E''E''E'}$	24.732	$d_{\Gamma \ \ \bar{K} \ \ K}^{B_{2g}E'E'}$	−41.699
$d_{\Gamma \ \ \bar{K} \ \ K}^{E_{2g}A_1'E'}$	−455.829	$d_{\Gamma \ \ \bar{K} \ \ K}^{E_{2g}A_2'E'}$	−50.356
$d_{\Gamma \ \ \bar{K} \ \ K}^{E_{2g}E'E'}$	204.211	$d_{\Gamma \ \ \bar{K} \ \ K}^{E_{2g}E''E''}$	−32.416

respect to $u_{\mathbf{q}_1}^{(\alpha_1, a_1)} \ldots u_{\mathbf{q}_\mathcal{N}}^{(\alpha_\mathcal{N}, a_\mathcal{N})}$ can be determined from evaluating the corresponding derivatives with respect to the stars. Group theoretically, one is left with the problem of forming symmetric direct products [87,88] of a set of stars [28,36]. As discussed in Sec. I B, this is a solved problem, though it is still nontrivial to execute at arbitrary order $\mathcal{N}$, as we have. Explicit results are illustrated for graphene (see Tables I and Ref. [15] SIII) and rock salt (see Appendix A).

For a given allowed derivative with respect to $u_{\mathbf{q}_1}^{(\alpha_1, a_1)} \ldots u_{\mathbf{q}_\mathcal{N}}^{(\alpha_\mathcal{N}, a_\mathcal{N})}$, the α_i associated with each $\mathbf{q}_i$ must be stored. We introduce the set $\tilde{\mathcal{A}}_Q$ which contains the allowed tuples of irreducible representations α_i associated with $\mathbf{q}_i$, where the ordering of the tuple corresponds to $\mathbb{S}(Q)$. For the example of graphene with $Q = [\Gamma, \bar{K}, K]$, we have

$$\tilde{\mathcal{A}}_{[\Gamma, \bar{K}, K]} = \{(E, E, E), (E, E, A_1), (E, E, A_2)\}. \quad (20)$$

We now define relevant variables to count the total number of identity representations. While $\tilde{\mathcal{A}}_Q$ contains all allowed symmetric products $\boldsymbol{\alpha}$, each will result in one or more identity representations; which is counted with the variable $n_{\boldsymbol{\alpha}}^Q$. The number of identity representations for a given Q is then $n_{ir}^Q = \sum_{\boldsymbol{\alpha} \in \tilde{\mathcal{A}}_Q} n_{\boldsymbol{\alpha}}^Q$, and $n_{ir}^Q = n_{ir}^{\tilde{S}_Q}$ for all $Q \in \tilde{S}$. The total number of irreducible derivatives can then be found as

$$n_{ir}^{\hat{S}_{BZ}} = \sum_{Q \in \tilde{Q}_{IBZ}} n_{ir}^Q = \sum_{\tilde{S} \in \tilde{S}_{BZ}} n_{ir}^{\tilde{S}}. \quad (21)$$

A final point is that time reversal symmetry can be employed in conjunction with space group symmetry to determine if space group irreducible derivatives can have a phase convention which ensures that they are purely real numbers (or purely imaginary), and this will influence the counting in Eq. (21). All applications in this paper have purely real (or imaginary) irreducible derivatives.

F. Homogeneity and isotropy of space

In addition to space group symmetry and permutation of derivative indices, the potential will also conserve total linear and angular momentum. The former implies that an arbitrary shift of the system will leave all derivatives of the

Born-Oppenheimer surface invariant [38,39]; and this is referred to as the acoustic sum rule in the context of a Taylor series in the real-space basis. The acoustic sum rules can be quite challenging for real-space Taylor series approaches to enforce [69,84,85]. To the contrary, when working with space group irreducible derivatives, and even simply translation group irreducible derivatives, the acoustic sum rules are automatically satisfied to all order by construction. Moreover, each irreducible derivative will individually satisfy the acoustic sum rule, and therefore the acoustic sum rule does not redistribute error among different irreducible derivatives. This is true for any translation group [see Eq. (6)], irrespective of its size. The only care that is needed occurs when the acoustic modes, at the Γ point, are a repeating irreducible representation, and then one should ensure that they are orthogonalized to the modes of the same symmetry; which is trivial to enforce by construction. Given that space group irreducible derivatives are invariant to supercell size, and that the acoustic sum rules are automatically satisfied, there are major incentives to work purely with space group irreducible derivatives.

In the case of conservation of total angular momentum, an arbitrary global rotation will leave the potential unchanged; and enforcing this in the limit of small rotations will link a given order of real-space derivatives to infinite range, in addition to linking them to the next order [39]. However, this does not impart any constraints on the space group irreducible derivatives within a FTG, given that the basis of the FTG does not describe pure rotation. However, the constraint may be placed within the method of Fourier interpolation (see Sec. II H), which interpolates the irreducible derivatives to the infinite lattice; here, free infinitesimal rotation can be enforced. In summary, isotropy of free space is not a consideration when extracting space group irreducible derivatives.

G. Taylor series of V in symmetrized variables

Having accounted for all symmetries, we are now in a position to write the Taylor series purely in terms of space group irreducible derivatives. We will label a given irreducible derivative at order $\mathcal{N}$ as $^jd_{\mathbf{q}_1 \cdots \mathbf{q}_\mathcal{N}}^{\alpha_1 \cdots \alpha_\mathcal{N}}$, where $\mathbf{q}_i$ is the ith element of $\mathbb{S}(Q)$, α_i is the ith element of $\boldsymbol{\alpha}$ (where $\boldsymbol{\alpha} \in \tilde{\mathcal{A}}_Q$), and $j \in [1, n_{\boldsymbol{\alpha}}^Q]$ labels repeating instances of an identity representation within a given symmetric product. We will also use a compressed notation $^jd_Q^{\boldsymbol{\alpha}}$. A given derivative of the Born-Oppenheimer surface can be written in terms of the irreducible derivatives as

$$\frac{\partial^{\mathcal{N}} V}{\prod_i^{\mathcal{N}} \partial u_{\mathbf{q}_i}^{(\alpha_i, a_i)}} = \sum_j {}^j\theta_{a_1 \ldots a_\mathcal{N}}^{\alpha_1 \ldots \alpha_\mathcal{N}}(\mathcal{Q}) \, {}^jd_{\mathbf{q}_1 \ldots \mathbf{q}_\mathcal{N}}^{\alpha_1 \ldots \alpha_\mathcal{N}}$$

$$= D_{\mathcal{Q}}^{(\alpha_1, a_1) \ldots (\alpha_\mathcal{N}, a_\mathcal{N})}, \quad (22)$$

where $\mathbf{q}_i \in \mathcal{Q}$, a_i is a given row of the α_i irreducible representation, $\theta_{a_1 \ldots a_\mathcal{N}}^{\alpha_1 \ldots \alpha_\mathcal{N}}(\mathcal{Q})$ are the Clebsch-Gordon (CG) coefficients of the direct product (DP) representation, the left superscript j is a label for repeating instances of a given identity representation, and the symbol D is used for the derivative of the potential with respect to irreducible representations of the displacements. The distinction between D and d should

be appreciated, as the latter only depends on irreducible representations α_i and *not* the rows of the irreducible representations a_i. Our convention for the DP CG coefficients is to start with the normalized CG coefficients of the symmetric direct product (SDP) representation, rescale the SDP CG by $\sqrt{n}$, where n is the smallest positive integer that produces the smallest number of radical SDP CG coefficients, and convert to the DP CG coefficients.

The Taylor series of the potential energy, per unit cell, is then written for a given FTG and order as

$$V_{\hat{\mathbf{S}}_{\mathrm{BZ}}}^{(\mathcal{N})} = \frac{1}{\mathcal{N}!} \sum_{\mathcal{Q}\in\tilde{\mathcal{Q}}_{\mathrm{BZ}}} \sum_{\substack{\alpha_1\dots\alpha_{\mathcal{N}} \\ a_1\dots a_{\mathcal{N}}}} D_{\mathcal{Q}}^{(\alpha_1,a_1)\dots(\alpha_{\mathcal{N}},a_{\mathcal{N}})} \prod_{i=1}^{\mathcal{N}} u_{\mathbf{q}_i}^{(\alpha_i,a_i)} = \frac{1}{\mathcal{N}!} \sum_{\substack{\mathcal{Q}\in\tilde{\mathcal{Q}}_{\mathrm{IBZ}} \\ \boldsymbol{\alpha}\in\tilde{\mathcal{A}}_{\mathcal{Q}},\, j}} {}^j d_{\mathcal{Q}}^{\boldsymbol{\alpha}} \mathcal{P}_{\mathcal{Q}}^{\boldsymbol{\alpha}} \sum_{Q'\in\bar{\mathcal{S}}_{\mathcal{Q}}} \sum_{a_1\dots a_{\mathcal{N}}} {}^j\theta_{a_1\dots a_{\mathcal{N}}}^{\alpha_1\dots\alpha_{\mathcal{N}}}(Q') \prod_{i=1}^{\mathcal{N}} u_{\mathbf{q}_i'}^{(\alpha_i,a_i)}, \quad (23)$$

where $\mathcal{P}_{\mathcal{Q}}^{\boldsymbol{\alpha}}$ is the number of permutations of $[(\alpha_i,\mathbf{q}_i)|i\in[1,\mathcal{N}]]$ with i denoting the ith element of $\boldsymbol{\alpha}$ and $\mathbb{S}(Q)$, and ${}^j\theta_{a_1\dots a_{\mathcal{N}}}^{\alpha_1\dots\alpha_{\mathcal{N}}}(Q') = {}^j\theta_{a_1\dots a_{\mathcal{N}}}^{\alpha_1\dots\alpha_{\mathcal{N}}}(\mathbb{S}(Q'))$. For the specific case of in-plane displacements in graphene at $\mathcal{N}=3$ with $\hat{\mathbf{S}}_{\mathrm{BZ}}=\hat{\mathbf{S}}_K$, we have

$$V_{\hat{\mathbf{S}}_K}^{(3)} = \frac{1}{6} d_{\Gamma\Gamma\Gamma}^{E_2 E_2 E_2} \left(3 u_{\Gamma}^{E_2^0} u_{\Gamma}^{E_2^0} u_{\Gamma}^{E_2^1} - u_{\Gamma}^{E_2^1} u_{\Gamma}^{E_2^1} u_{\Gamma}^{E_2^1}\right) + d_{\Gamma\bar{K}K}^{EEE}\left(u_{\Gamma}^{E^0} u_{\bar{K}}^{E^0} u_K^{E^1} + u_{\Gamma}^{E^0} u_{\bar{K}}^{E^1} u_K^{E^0} + u_{\Gamma}^{E^1} u_{\bar{K}}^{E^0} u_K^{E^0} - u_{\Gamma}^{E^1} u_{\bar{K}}^{E^1} u_K^{E^1}\right)$$

$$+ d_{\Gamma\bar{K}K}^{EEA_1}\left(u_K^{A_1}\left(u_{\Gamma}^{E^0} u_{\bar{K}}^{E^0} + u_{\Gamma}^{E^1} u_{\bar{K}}^{E^1}\right) + \mathrm{c.c.}\right) + d_{\Gamma\bar{K}K}^{EEA_2}\left(u_K^{A_2}\left(u_{\Gamma}^{E^0} u_{\bar{K}}^{E^1} - u_{\Gamma}^{E^1} u_{\bar{K}}^{E^0}\right) + \mathrm{c.c.}\right) + \frac{1}{6} d_{KKK}^{A_1 A_1 A_1}\left(u_K^{A_1} u_K^{A_1} u_K^{A_1} + \mathrm{c.c.}\right)$$

$$+ \frac{1}{2} d_{KKK}^{A_1 A_2 A_2}\left(u_K^{A_1} u_K^{A_2} u_K^{A_2} + \mathrm{c.c.}\right) + \frac{1}{2} d_{KKK}^{EEA_1}\left(u_K^{A_1}\left(u_K^{E^0} u_K^{E^0} + u_K^{E^1} u_K^{E^1}\right) + \mathrm{c.c.}\right) + \frac{1}{6} d_{KKK}^{EEE}\left(\left(3 u_K^{E^0} u_K^{E^0} u_K^{E^1} - u_K^{E^1} u_K^{E^1} u_K^{E^1}\right) + \mathrm{c.c.}\right),$$

$$(24)$$

where c.c. indicates the complex conjugate of the preceding term, superscripts of irreducible representations indicate a given row of a multidimensional irreducible representation, and we have used C_{3v} labels for the little group of K for convenience; as opposed to D_{3h}, which is needed when including out-of-plane displacements. The values of the above derivatives can be found in Table I, and the approaches to computing them are discussed in Sec. III. We emphasize that to third order, *any possible* in-plane displacement within $\hat{\mathbf{S}}_K$ is purely characterized by the eight real irreducible derivatives shown in Eq. (24) in addition to the four in-plane irreducible derivatives at second order (see Table I).

H. Fourier interpolation

Given a set of irreducible derivatives defined over some FTG, one may interpolate to a different FTG or the infinite lattice; and this can be achieved using Fourier Interpolation (FI) [10,11]. Such trigonometric interpolations have a long history in physics, dating back to the beginning of classical mechanics [89]. We emphasize that FI is not unique, and one could supply additional information, such as the elastic constants, to improve the FI. Beyond second order, the only description of FI we are aware of is the treatment of third order in Ref. [62]. In the present work, we need a FI scheme for arbitrary order, and therefore we implement the most straightforward generalization of the usual FI at second order [11,62]; which amounts repacking the force tensor into the Wigner-Seitz cell.

Here we outline the various steps in our FI approach. First, the dynamical tensor needs to be rotated to a common basis at each $\mathcal{Q}\in\tilde{\mathcal{Q}}_{\mathrm{BZ}}$, which is chosen as the naive basis labeled by each atom and Cartesian displacement:

$$D_{\mathcal{Q}}'^{i_1,\dots,i_{\mathcal{N}}} = \sum_{\ell_1,\dots,\ell_{\mathcal{N}}} \prod_{j=1}^{\mathcal{N}} U_{\mathbf{q}_j}^{i_j \ell_j} D_{\mathcal{Q}}^{\ell_1,\dots,\ell_{\mathcal{N}}}, \quad (25)$$

where $\hat{\mathbf{U}}_{\mathbf{q}}$ are the matrices that transform from the symmetrized basis under the little group of $\mathbf{q}$ to the naive basis (provided for graphene in Ref. [15], Table SII), and the index i_j is a two tuple containing both an atom and displacement label, while ℓ_j is a two tuple labeling a row of an irreducible representation of the little group of $\mathbf{q}_j$. Subsequently, the dynamical tensor can be Fourier transformed to obtain the force tensor:

$$\Phi_{\mathcal{T}} = \frac{1}{n_q^{\mathcal{N}-1}} \sum_{\mathcal{Q}\in\tilde{\mathcal{Q}}_{\mathrm{BZ}}} \boldsymbol{D}'_{\mathcal{Q}} e^{i2\pi\mathrm{Tr}(\hat{\mathcal{Q}}\hat{\mathcal{T}}^{\mathsf{T}})}, \quad (26)$$

where $\mathbf{t}\in\mathcal{T}$ and $\mathcal{T}\in\tilde{\mathcal{T}}_{\mathrm{BZ}}$. At this point, $\{\Phi_{\mathcal{T}}|\mathcal{T}\in\tilde{\mathcal{T}}_{\mathrm{BZ}}\}$ can then be used to predict $\boldsymbol{D}_{\mathcal{Q}}$ at an arbitrary $\mathcal{Q}$ point. However, such an interpolation does not guarantee point symmetry for $\mathcal{Q}\notin\tilde{\mathcal{Q}}_{\mathrm{BZ}}$, and therefore an additional transformation is needed. The basic approach is to repack $\Phi_{\mathcal{T}}$, defined over $\tilde{\mathcal{T}}_{\mathrm{BZ}}$, into the corresponding Wigner-Seitz cell. To do so, a map $\mathbb{W}_{\mathcal{T}}^{a_1\cdots a_{\mathcal{N}}}$, where a_i label one of the n_a basis atoms in the primitive unit cell, must be created from the translation points $\tilde{\mathcal{T}}_{\mathrm{BZ}}^{\mathrm{WS}}$ defined over the WS BvK supercell to the conventional BvK supercell $\tilde{\mathcal{T}}_{\mathrm{BZ}}$.

In order to build $\mathbb{W}_{\mathcal{T}}^{a_1\cdots a_{\mathcal{N}}}$, we begin by building $w_{\mathbf{t}}^{ij}$, which is the corresponding map from $\tilde{t}_{\mathrm{BZ}}$ to $\tilde{t}_{\mathrm{BZ}}^{\mathrm{WS}}$. The process of deducing this map is related to finding the Wigner-Seitz cell associated with $\hat{\mathbf{S}}_{\mathrm{BZ}}$, and this is illustrated in the case of $\hat{\mathbf{S}}_{\mathrm{BZ}}=\hat{\mathbf{S}}_K$ in graphene (see Fig. 2). Figure 2(a) contains a schematic of the graphene lattice, with each basis atom labeled by the translation, in lattice coordinates, of the infinite lattice. The FTG $\hat{\mathbf{S}}_K$ is illustrated in red, while the corresponding WS cell is illustrated in blue and green for centerings on the first and second carbon atom, respectively. Figure 2(b) retains only the six carbon atoms associated with $\hat{\mathbf{S}}_K$, and the task is to shift all of these atoms by any translation $\{\mathbf{t}\hat{\mathbf{S}}_K|\mathbf{t}\in\mathbb{Z}^d\}$ that maps the atom into or onto the boundary of the WS cell; and each atom may be shifted by more than one translation. Figures 2(c) and
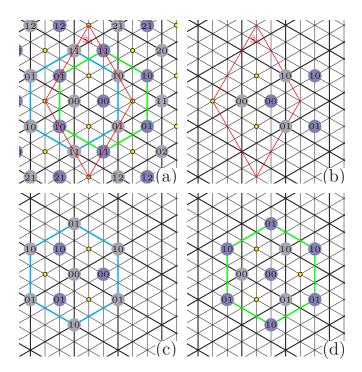
FIG. 2. (a) Schematic of the graphene crystal structure, where yellow hexagons represent lattice points and circles represent carbon atoms; and each carbon atom is labeled by two integers which correspond to a translation in lattice coordinates. The $\hat{\mathbf{S}}_K$ supercell is shown in red, and the corresponding WS cell is shown in blue and green for a centering on the first and second carbon atom, respectively. (b) Schematic showing $\mathbf{t} \in \tilde{t}_{\mathrm{BZ}}$ for $\hat{\mathbf{S}}_{\mathrm{BZ}} = \hat{\mathbf{S}}_K$ along with the corresponding basis atoms. (c) Schematic showing how the basis atoms are translated back into the WS cell using some vector $\mathbf{t}\hat{\mathbf{S}}_K\hat{\mathbf{a}}$, with $\mathbf{t} \in \mathbb{Z}^d$, where the centering of the WS cell is on the first carbon atom. (d) Same as (c) but with the WS cell centered on the second carbon atom.

2(d) show the result of this for the two different WS cells, and the resulting map can be deduced by comparing to Fig. 2(a):

$$w_{\mathbf{0}}^{i,i} = \{\mathbf{0}\}, \qquad\qquad w_{\mathbf{0}}^{i,j} = \{\mathbf{0}\},$$

$$w_{\mathbf{t}_a}^{i,i} = \{\mathbf{t}_a, (0, \bar{1}), (\bar{1}, 1)\}, \qquad w_{\mathbf{t}_a}^{0,1} = \{(0, \bar{1})\},$$

$$w_{\mathbf{t}_b}^{i,i} = \{\mathbf{t}_b, (\bar{1}, 0), (1, \bar{1})\}, \qquad w_{\mathbf{t}_b}^{0,1} = \{(\bar{1}, 0)\},$$

$$w_{\mathbf{t}_b}^{1,0} = \{\mathbf{t}_b\}, \qquad\qquad w_{\mathbf{t}_a}^{1,0} = \{\mathbf{t}_a\}. \qquad (27)$$

Clearly, $w_{\mathbf{t}}^{i,i}$ is purely a property of the lattice, with $\tilde{t}_{\mathrm{BZ}}^{\mathrm{WS}} = \bigcup_{\mathbf{t} \in \tilde{t}_{\mathrm{BZ}}} w_{\mathbf{t}}^{i,i}$, while $w_{\mathbf{t}}^{i,j}$ ($i \neq j$) will depend on the relative positions of the basis atoms. Having deduced $\{w_{\mathbf{t}}^{i,j} | \mathbf{t} \in \tilde{t}_{\mathrm{BZ}}\}$, any element $\mathbb{W}_{\mathcal{T}}^{a_1 \cdots a_{\mathcal{N}}}$ can now straightforwardly be constructed at an arbitrary $\mathcal{N}$ within $\hat{\mathbf{S}}_K$. For example, at $\mathcal{N} = 3$, one case is

$$\mathbb{W}_{(\mathbf{0}, \mathbf{t}_a, \mathbf{t}_b)}^{0,0,1} = \{(\mathbf{0}, \mathbf{t}_a, (\bar{1}, 0)),$$
$$(\mathbf{0}, (0, \bar{1}), (\bar{1}, 0)), (\mathbf{0}, (\bar{1}, 1), (\bar{1}, 0))\}. \qquad (28)$$

Once the map is obtained, $\Phi_{\mathcal{T}}^{\mathrm{WS}}$ can be constructed:

$$\Phi_{\mathcal{T}'}^{WS,(a_1,\alpha_1)\cdots(a_{\mathcal{N}},\alpha_{\mathcal{N}})} = \left| \mathbb{W}_{\mathcal{T}}^{a_1\cdots a_{\mathcal{N}}} \right|^{-1} \Phi_{\mathcal{T}}^{(a_1,\alpha_1)\cdots(a_{\mathcal{N}},\alpha_{\mathcal{N}})}, \qquad (29)$$
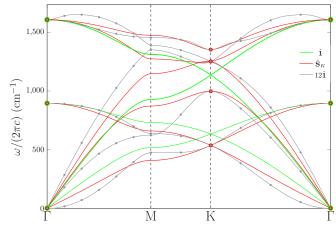

FIG. 3. Phonons of graphene within DFT for $\hat{\mathbf{S}}_{\mathrm{BZ}} = \hat{\mathbf{1}}$, $\hat{\mathbf{S}}_K$, and $12\hat{\mathbf{1}}$, where data points are direct computational measurements and lines are Fourier interpolation. The irreducible derivatives for $\hat{\mathbf{1}}$ and $\hat{\mathbf{S}}_K$ are shown in Table I; and the corresponding frequencies are obtained, in units of s^{-1}, as $\omega_{\mathbf{q}}^{\alpha} = \sqrt{d_{\tilde{\mathbf{q}}\mathbf{q}}^{\alpha\alpha}/m}$, where $m = 12.011 \cdot 1.0364 \times 10^{-28}$ eV s^2 Å^{-2} for carbon. The y axis plots $\omega_{\mathbf{q}}^{\alpha}/(2\pi c)$, where c is the speed of light in units of cm/s.

where $\mathcal{T}' \in \mathbb{W}_{\mathcal{T}}^{a_1 \cdots a_{\mathcal{N}}}$. Finally, an arbitrary $\mathcal{Q}$ can be constructed as

$$\boldsymbol{D}_{\mathcal{Q}} = \sum_{\mathcal{T} \in \tilde{\mathcal{T}}_{\mathrm{BZ}}^{\mathrm{WS}}} \Phi_{\mathcal{T}}^{\mathrm{WS}} e^{-i2\pi \mathrm{Tr}(\hat{\mathcal{Q}}\hat{\mathcal{T}}^{\mathsf{T}})}. \qquad (30)$$

This procedure has been straightforwardly executed on graphene up to $\mathcal{N} = 5$ (see Sec. IV).

As an illustration, we provide the Fourier interpolation of graphene at second order for $\hat{\mathbf{S}}_{\mathrm{BZ}} = \hat{\mathbf{1}}$, $\hat{\mathbf{S}}_{\mathrm{BZ}} = \hat{\mathbf{S}}_K$, and $\hat{\mathbf{S}}_{\mathrm{BZ}} = 12\hat{\mathbf{1}}$ (see Fig. 3). The data points denote frequencies at specific $\mathbf{q}$ which result from direct measurement, while the lines are the result of the Fourier interpolation, and it is clear that all symmetries are satisfied. We emphasize that only the data points are robust, and the lines are only reliable for a sufficiently large FTG. Given that there are no repeating irreducible representation for $\hat{\mathbf{S}}_{\mathrm{BZ}} = \hat{\mathbf{1}}$ and $\hat{\mathbf{S}}_{\mathrm{BZ}} = \hat{\mathbf{S}}_K$, the phonon frequencies at the irreducible representations of the FTG can be obtained without any matrix diagonalization (see caption of Fig. 3).

III. FINITE DISPLACEMENT METHODOLOGY

A. Statement of problem

Having developed a Taylor series purely in terms of space group irreducible derivatives at order $\mathcal{N}$, we now turn to the problem of how to compute these derivatives using finite displacements; while exploiting perturbative derivatives (e.g., Hellman-Feynman forces) up to order η, with $\eta < \mathcal{N}$, that the first-principles approach may provide. We refer to the order η perturbative derivatives as PD$_\eta$.

Generically speaking, we define a finite displacement method as any method which explicitly moves the nuclei and fully computes the electronic structure. There are now many techniques which use a first-principles molecular dynamics trajectory as a source of data from which to fit [46,47,90], and this would fall under the category of a finite displacement

approach. Furthermore, those approaches extracting third-order derivatives from a molecular dynamics trajectory could obviously exploit our hierarchical supercell approach outlined in Sec. III B, though we do not pursue such a program in this work because we believe fitting tens to thousands of parameters simultaneously should always be a method of last resort. Instead, we seek to use central finite difference, where the only simultaneous fitting involved is that of a quadratic function which has two parameters, and order $\mathcal{N}$ derivatives are isolated from all other orders.

We define two finite difference based approaches at competing extremes: the lone irreducible derivative (LID) and the bundled irreducible derivative (BID) approach. The LID approach measures the smallest possible number of irreducible derivatives simultaneously, sacrificing efficiency for accuracy, while BID simultaneously measures the maximum number of irreducible derivatives that the perturbative derivatives will allow, prioritizing efficiency over accuracy. A spectrum possibilities exists between these two approaches, though we focus on these two extremes. Both LID and BID can be executed in a single-supercell approach, performing all calculations within the BvK supercell $\hat{\mathbf{S}}_{\text{BZ}}$, or a hierarchical supercell approach, where each irreducible derivative is measured in the smallest corresponding supercell allowed by group theory. We proceed by first outlining how to derive the smallest supercell that will accommodate an arbitrary set of $\mathcal{N}$ waves $\mathbf{q} \in \mathcal{Q}$. We emphasize that this question is generic to any sort of waves within the lattice.

B. Minimum supercell problem

The following unresolved problem is of utmost importance in any finite displacement approach: given $\mathcal{Q}$, find the smallest possible supercell, denoted $\hat{\mathbf{S}}_{\mathcal{Q}}$, that accommodates all $\mathcal{N}$ vectors $\mathbf{q} \in \mathcal{Q}$. Mathematically, we demand that all $\mathbf{q} \in \mathcal{Q}$ are identity representations of the supercell, $\hat{\mathcal{Q}}\hat{\mathbf{S}}_{\mathcal{Q}}^{\mathsf{T}} \in \mathbb{Z}^{(\mathcal{N}, d)}$, with the constraint that $|\det(\hat{\mathbf{S}}_{\mathcal{Q}})|$ is a minimum. Recall that $\sum_{\mathbf{q} \in \mathcal{Q}} \mathbf{q} \in \mathbb{Z}^d$, which demands that a supercell which accommodates any $\mathcal{N} - 1$ of the $\mathbf{q} \in \mathcal{Q}$ will automatically accommodate the remaining $\mathbf{q}$. Therefore we are free to remove any one row from $\hat{\mathcal{Q}}$. Furthermore, it is useful to work with a purely integer equation, so we define a new matrix $\hat{\mathcal{Q}}'$, which is obtained by removing any row from $\hat{\mathcal{Q}}$ and multiplying by L; where L is the least common denominator for all components of $\mathbf{q} \in \mathcal{Q}$. The matrix $\hat{\mathcal{Q}}'$ is a $(\mathcal{N} - 1) \times d$ matrix of integers, and the commensuration requirement becomes $\hat{\mathcal{Q}}' \hat{\mathbf{S}}_{\mathcal{Q}}^{\mathsf{T}}(\text{mod } L) = \hat{\mathbf{0}}$, where $\hat{\mathbf{0}}$ is a $(\mathcal{N} - 1) \times d$ dimensional zero matrix. Finally, the mathematical requirement for a valid $\hat{\mathbf{S}}_{\mathcal{Q}}$ is

$$\hat{\mathbf{S}}_{\mathcal{Q}} \in \underset{\hat{\mathbf{n}} \in \mathbb{Z}^{(d,d)}}{\arg \min}\{|\hat{\mathbf{n}}| : \hat{\mathcal{Q}}' \hat{\mathbf{n}}^{\mathsf{T}}(\text{mod } L) = \hat{\mathbf{0}}, |\hat{\mathbf{n}}| \geqslant 1\}. \quad (31)$$

Performing this minimization is achieved by constructing the modulo L kernel of $\hat{\mathcal{Q}}'$, which is obtained by bringing $\hat{\mathcal{Q}}'$ into Smith normal form (SNF) [91], denoted $\hat{\mathbf{N}}$; and this is achieved via elementary row and column operations:

$$\hat{\mathbf{N}} = \hat{\mathbf{R}}\hat{\mathcal{Q}}'\hat{\mathbf{C}}, \quad (32)$$

where $\hat{\mathbf{N}}$ is a $(\mathcal{N} - 1) \times d$ diagonal matrix of integers, $\hat{\mathbf{R}}$ is a $(\mathcal{N} - 1) \times (\mathcal{N} - 1)$ unimodular matrix of integers obtained from a sequence of elementary row transformations, and $\hat{\mathbf{C}}$ is a $d \times d$ unimodular matrix of integers obtained from a sequence of elementary column transformations.

The modulo L kernel of $\hat{\mathbf{N}}$ can be formed as

$$\ker(\hat{\mathbf{N}})_i = \frac{L}{\gcd(L, G_{ii})}\mathbf{e}_i, \quad \begin{array}{l} G_{ii} = N_{ii} \text{ if } i \leqslant \mathcal{N} - 1, \\ G_{ii} = L \text{ if } i > \mathcal{N} - 1, \end{array} \quad (33)$$

where $\mathbf{e}_i$ is a unit vector in $\mathbb{Z}^d$ and the matrix $\ker(\hat{\mathbf{N}})$ consists of d column vectors $\ker(\hat{\mathbf{N}})_i \in \mathbb{Z}^d$. Therefore we have

$$\hat{\mathbf{R}}\hat{\mathcal{Q}}'\hat{\mathbf{C}} \ker(\hat{\mathbf{N}})(\text{mod } L) = \hat{\mathbf{0}}. \quad (34)$$

Finally, we can then define a given basis vector of the kernel of $\hat{\mathcal{Q}}'$, and the resulting supercell

$$\ker(\hat{\mathcal{Q}}') = \hat{\mathbf{C}} \ker(\hat{\mathbf{N}}), \quad \hat{\mathbf{S}}_{\mathcal{Q}} = \ker(\hat{\mathcal{Q}}')^{\mathsf{T}}, \quad (35)$$

though it should be emphasized that this supercell is not unique and may be reshaped. Most importantly, the multiplicity of the supercell is

$$\det(\hat{\mathbf{S}}_{\mathcal{Q}}) = \frac{L^d}{\prod_{i=1}^{d} \gcd(L, G_{ii})}. \quad (36)$$

We refer to Eq. (36) as the minimum supercell multiplicity (MSM) equation. Given that calculating the Smith normal form is computationally inexpensive for $d \leqslant 3$ at any realistic $\mathcal{N}$, the MSM equation can be efficiently evaluated. In order to clearly illustrate this approach, a worked example is provided in Appendix C.

Under certain restrictions, the largest necessary supercell multiplicity of a given FTG can be determined from Eq. (36) *a priori*. For any FTG of an arbitrary d-dimensional crystal at $\mathcal{N} = 2$ (i.e. phonons), in addition to FTG's corresponding to $\hat{\mathbf{S}}_{\text{BZ}} = n\hat{\mathbf{1}}$, where $n \in \mathbb{Z}^+$, at arbitrary order $\mathcal{N}$, the largest necessary supercell multiplicity is $L_m^{\min(\mathcal{N}-1,d)}$ (see Sec. II B for L_m). Restated in equations, we have

$$\mathcal{N} = 2 \vee \hat{\mathbf{S}}_{\text{BZ}} = n\hat{\mathbf{1}} \Rightarrow \max_{\mathcal{Q} \in \tilde{\mathcal{Q}}_{\text{BZ}}} |\hat{\mathbf{S}}_{\mathcal{Q}}| = L_m^{\min(\mathcal{N}-1,d)}. \quad (37)$$

The above can be proven in two parts. For $\mathcal{N} = 2$, an arbitrary $\mathbf{q} = (q_1/L_m, q_2/L_m, \ldots, q_d/L_m)$, where $0 \leqslant q_i < L_m$ and $q_i \in \mathbb{Z}$, and we have $N_{11} = \gcd(q_1, \ldots, q_d)$. Since $\hat{\mathcal{Q}}'$ is a single row, the multiplicity is

$$\det(\hat{\mathbf{S}}_{\mathcal{Q}}) = \frac{L_m}{\gcd(L_m, N_{11})} = \frac{L_m}{\gcd(L_m, q_1, \ldots, q_d)}. \quad (38)$$

Given that the minimum of the denominator is 1, the maximum multiplicity is L_m. For the case of $\hat{\mathbf{S}}_{\text{BZ}} = n\hat{\mathbf{1}}$, at arbitrary $\mathcal{N}$, we have $L_m = n$ and therefore $\mathbf{q}_i = (q_{i,1}/n, \ldots, q_{i,d}/n)$; where $q_{i,j} \in [0, n-1]$ and $q_{i,j} \in \mathbb{Z}$. Then, we have

$$\det(\hat{\mathbf{S}}_{\mathcal{Q}}) = \frac{n^{\min(\mathcal{N}-1,d)}}{\prod_{i=1}^{\min(\mathcal{N}-1,d)} \gcd(n, G_{ii})}. \quad (39)$$

The worst case is $\gcd(n, G_{ii}) = 1$, yielding a maximum multiplicity $n^{\min(\mathcal{N}-1,d)}$.

Equation (37) has far reaching implications which should be appreciated. For typical materials systems (i.e., $d = 1, 2, 3$), Eq. (37) dictates that phonons can always be obtained

from a collection of supercells of multiplicity L_m, as was only recently realized [76]. Moreover, for three dimensional materials with a FTG of $\hat{\mathbf{S}}_{BZ} = n\hat{\mathbf{1}}$, cubic terms can always be obtained from a collection of supercells of maximum multiplicity n^2, proving that the BvK supercell can always be avoided for cubic terms in this common scenario.

Given that our approach produces the required supercells, there is no need to use a dedicated algorithm, such as Ref. [92], to generate all distinct supercells of a given multiplicity (i.e., all distinct Hermite normal forms) and determine if $\mathcal{Q}$ is commensurate, as executed in the special case of $\mathcal{N} = 2$ in Ref. [76].

C. Central finite difference

Central finite difference (CFD) is the method of choice in this study for computing an arbitrary derivative using finite displacements. The main virtue of CFD is that the error is a quadratic function of the discretization parameter Δ. Given perturbative derivatives of order η (where $\eta < \mathcal{N}$), denoted PD_η, the order $\mathcal{N}' = \mathcal{N} - \eta$ derivatives of the PD_η from CFD is obtained as the intercept of the following *even* function (the indices of $u_{\mathbf{t}}^{(b,\beta)}$, $u_{\mathbf{q}}^{(\alpha,a)}$ are compressed to u_i for brevity):

$$V_{u_1 \dots u_{\mathcal{N}'}}^{u_1' \dots u_\eta'}(\Delta) = \sum_{n_1, \cdots, n_{\mathcal{N}'} = (-1,1)} \frac{\left(\prod_{i=1}^{\mathcal{N}'} n_i\right) V^{u_1' \dots u_\eta'}(\{n_i \Delta\})}{2^{\mathcal{N}'} \Delta^{\mathcal{N}'}}$$

$$= \frac{\partial^{\mathcal{N}'} V^{u_1' \dots u_\eta'}}{\prod_{i=1}^{\mathcal{N}'} \partial u_i} + O(\Delta^2) + \cdots, \qquad (40)$$

where $V^{u_1' \dots u_\eta'}$ is a given perturbative derivative ($\eta = 0$ implies V, etc.), the variables $u_1 \dots u_{\mathcal{N}'}$ are the arguments of the order $\mathcal{N}'$ CFD derivatives, and Δ is a positive real number. Higher-order CFD derivatives of a given variable are obtained by repeating the same variable. A given Δ for an order $\mathcal{N}'$ derivative will require up to $2^{\mathcal{N}'}$ evaluations of $V^{u_1' \dots u_\eta'}$. The intercept of the Eq. (40) gives the value of the order $\mathcal{N}$ derivative of V, and CFD guarantees that the leading-order correction of an order $\mathcal{N}'$ derivative is comprised of the order $\mathcal{N}' + 2$ derivatives; which dictate the strength of the quadratic error tail (see Ref. [52] for additional details). Every evaluation of $V^{u_1' \dots u_\eta'}$ at a given Δ requires the numerical solution of some first-principles method (e.g., Kohn-Sham equation of DFT) which is subject to it's own discretization errors (e.g., plane-wave cutoff, etc.). Therefore, for sufficiently small Δ, the finite difference will be dominated by errors; while if Δ is too large, then the results will be beyond the quadratic regime. One needs to ensure that the quadratic regime is obtained such that a valid extrapolation $\Delta \to 0$ can be obtained: a practical but essential point. We will demonstrate that this quadratic extrapolation can typically be achieved even for $\mathcal{N}' = 4$ within DFT (i.e., fifth derivatives of the energy if the forces are being used).

Choosing the discretization grid is an interesting optimization problem in its own right, and we aim for simplicity in this work; given that the current status quo at $\mathcal{N}' = 1$ and even sometimes $\mathcal{N}' = 2$ is simply choosing a single delta based on experience. At least three Δ would be needed to compute an error associated with fitting a quadratic. In this work, we typically compute up to fifteen Δ for a given

derivative, which is normally excessive, but it allowed for the testing of various schemes for optimizing the quadratic fit. Typical ranges of Δ for force derivatives ($\eta = 1$) were $\Delta = 0.005$–0.05 Å for $\mathcal{N}' = 1$; $\Delta = 0.01 - 0.1$ Å for $\mathcal{N}' = 2$; and $\Delta = 0.01$–0.15 Å for $\mathcal{N}' = 3, 4$. Given $V_{u_1 \dots u_{\mathcal{N}'}}^{u_1' \dots u_\eta'}(\Delta)$ evaluated over some set of N different Δ, we need to choose which points to use in the least squares fit of the quadratic error tail. To do so, we construct the least squares fit for all sets of Δ obtained from choosing n from N, where $n \in [4, N]$. Clearly, the smallest number of points will always deliver the smallest error, so we choose our metric to be the standard error of the fit divided by the number of points used in the fit. We reiterate that there are many different schemes one can choose, and in some situations it will suffice to choose a single Δ, such as some $\mathcal{N}' = 1$ derivatives, but it is difficult to know *a priori*. An illustration of the result of choosing the quadratic error tail can be seen in Fig. 4, which will be discussed in Sec. III D.

Hereafter, we refer to the determination of all derivatives associated with a given choice $u_1 \dots u_{\mathcal{N}'}$ as a single "measurement" [i.e., evaluating Eq. (40) for some number of Δ with a fixed choice $u_1 \dots u_{\mathcal{N}'}$ and extrapolating $\Delta \to 0$], and this should not be confused with a single calculation; as the number of calculations is determined by the number of Δ and the specific basis vectors one chooses. Given that different practitioners will choose different numbers of Δ, the number of measurements is what should be compared when contrasting different methods of extracting all derivatives. Finally, it should be noted that the cost of obtaining n distinct Δ may be considered to be far less than performing n independent calculations, given that the wave function of the $(n-1)$th Δ can be used to seed the nth Δ at a great reduction in computational cost; and we exploit this.

D. Individually resolving irreducible derivatives: lone irreducible derivative approach

The first procedure we outline involves measuring a single irreducible derivative at a time, or as few as group theoretically possible, which we call the lone irreducible derivative (LID) approach. This approach encompasses the original frozen phonon approach [70], but we apply it under the most general conditions. We emphasize that LID specifically refers to irreducible derivatives of the space group, and not simply irreducible derivatives of the translation group. While the LID approach can be executed in either a single or hierarchical supercell approach, there would never be a reason to use the former, and therefore LID will always imply the use of a hierarchical supercell approach.

If the first-principles method to evaluate V does not provide any perturbative derivatives, then LID is a natural choice. While any complete basis can be employed at the same cost, directly probing a given irreducible derivative could help circumvent potential numerical problems. If perturbative derivatives PD_η are available, where $\eta < \mathcal{N}$, LID becomes an inefficient choice, as the most efficient possibility is to simultaneously measure a maximum number of irreducible derivatives at once (see Secs. III E and III F for the bundled irreducible derivative approaches). However, LID is still essential in that it should be the method of choice for the most
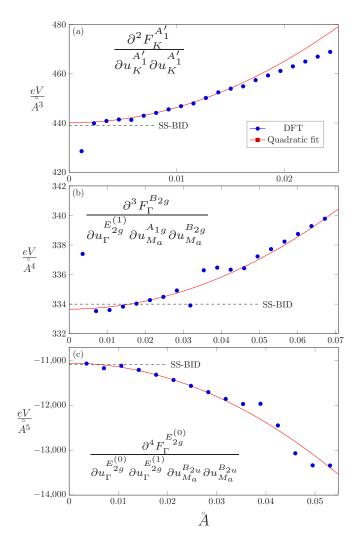
FIG. 4. All panels display central finite difference calculations as a function of Δ; points are calculated values while the red line is a quadratic fit to a subset of points chosen by the algorithm defined in Sec. III C. (a), (b), and (c) display a particular third-, fourth-, and fifth-order space group irreducible derivative, respectively, as obtained using the LID method with PD_1. The horizontal dashed lines show the result of the SS-BID method, where many irreducible derivative are simultaneously extracted.

accurate measurement of a *given* irreducible derivative. For example, when constructing a Taylor series of a particular mode associated with a structural phase transition, LID is the method of choice to ensure that each irreducible derivative is resolved as precisely as possible.

Given that the irreducible representations of the translation group are inherently complex numbers, $u_{\mathbf{q}}$ are in general complex. Therefore a unitary transformation to a real representation is needed:

$$u_{\mathbf{q}^c} = \frac{1}{\sqrt{2}}(u_{\mathbf{q}} + u_{\bar{\mathbf{q}}}), \quad u_{\mathbf{q}^s} = \frac{i}{\sqrt{2}}(u_{\bar{\mathbf{q}}} - u_{\mathbf{q}}). \quad (41)$$

We refer to this basis as the "real-q" representation, and it should be emphasized that these functions do not transform like irreducible representations of the translation group, though this is easily accounted for.

Given some irreducible derivative $d_{\mathbf{q}_1 \dots \mathbf{q}_{\mathcal{N}}}^{\alpha_1 \dots \alpha_{\mathcal{N}}}$, one needs to determine which corresponding real-q derivatives need to be measured. The first point to appreciate is that an irreducible derivative will in general be a complex number; though specific cases may be purely real due to the combination of time reversal and inversion symmetry, or if all $\{u_{\mathbf{q}} | \mathbf{q} \in Q\}$ are purely real (e.g., Γ point). We begin by considering the simplest case of PD_0. A complex derivative will require at least two measurements, in order to recover both the real and imaginary parts. For example, in order to determine the second order complex derivative $d_{\bar{\mathbf{q}}\mathbf{q}}^{\alpha_1 \alpha_2}$, where α_1 and α_2 are different instances of the same irreducible representation, then the chain rule in conjunction with Eq. (41) indicates that two derivatives must be measured, such as $V_{\mathbf{q}^c \mathbf{q}^c}^{\alpha_1 \alpha_2}$ and $V_{\mathbf{q}^c \mathbf{q}^s}^{\alpha_1 \alpha_2}$; where we use notation from Sec. II A and abbreviate $(\alpha_i, a_i) \to \alpha_i$, where a_i is a row of the irreducible representation determined from the symmetric product. If inversion symmetry is present, then a predetermined phase convention exists such that $d_{\bar{\mathbf{q}}\mathbf{q}}^{\alpha_1 \alpha_2}$ can be chosen to be real, and only $V_{\mathbf{q}^c \mathbf{q}^c}^{\alpha_1 \alpha_2}$ would need to be measured, as $V_{\mathbf{q}^c \mathbf{q}^s}^{\alpha_1 \alpha_2}$ would be zero by symmetry.

The same logic applies at higher order, though there are differences to consider. When using the real-q representation at higher order, it is possible that multiple irreducible derivatives will inherently be probed simultaneously. For example, consider the fourth-order derivative $d_{\bar{\mathbf{q}} \bar{\mathbf{q}} \mathbf{q} \mathbf{q}}^{\alpha_1 \alpha_2 \alpha_3 \alpha_4}$, where α_i are all distinct irreducible representations. In this case, any possible derivative $V_{\mathbf{q}^{r_1} \mathbf{q}^{r_2} \mathbf{q}^{r_3} \mathbf{q}^{r_4}}^{\alpha_1 \alpha_2 \alpha_3 \alpha_4}$, where $r_i \in \{c, s\}$, will inherently probe six complex irreducible derivatives:

$$
\begin{array}{ccc}
d_{\bar{\mathbf{q}} \bar{\mathbf{q}} \mathbf{q} \mathbf{q}}^{\alpha_1 \alpha_2 \alpha_3 \alpha_4}, & d_{\bar{\mathbf{q}} \bar{\mathbf{q}} \mathbf{q} \mathbf{q}}^{\alpha_1 \alpha_3 \alpha_2 \alpha_4}, & d_{\bar{\mathbf{q}} \bar{\mathbf{q}} \mathbf{q} \mathbf{q}}^{\alpha_1 \alpha_4 \alpha_2 \alpha_3}, \\
d_{\bar{\mathbf{q}} \bar{\mathbf{q}} \mathbf{q} \mathbf{q}}^{\alpha_3 \alpha_4 \alpha_1 \alpha_2}, & d_{\bar{\mathbf{q}} \bar{\mathbf{q}} \mathbf{q} \mathbf{q}}^{\alpha_2 \alpha_4 \alpha_1 \alpha_3}, & d_{\bar{\mathbf{q}} \bar{\mathbf{q}} \mathbf{q} \mathbf{q}}^{\alpha_2 \alpha_3 \alpha_1 \alpha_4}.
\end{array} \quad (42)
$$

Consequently, the chain rule dictates that six real-q derivatives must be measured, such as

$$
\begin{array}{ccc}
V_{\mathbf{q}^c \mathbf{q}^c \mathbf{q}^c \mathbf{q}^c}^{\alpha_1 \alpha_2 \alpha_3 \alpha_4}, & V_{\mathbf{q}^c \mathbf{q}^c \mathbf{q}^c \mathbf{q}^s}^{\alpha_1 \alpha_2 \alpha_3 \alpha_4}, & V_{\mathbf{q}^c \mathbf{q}^c \mathbf{q}^s \mathbf{q}^c}^{\alpha_1 \alpha_2 \alpha_3 \alpha_4}, \\
V_{\mathbf{q}^c \mathbf{q}^s \mathbf{q}^c \mathbf{q}^c}^{\alpha_1 \alpha_2 \alpha_3 \alpha_4}, & V_{\mathbf{q}^s \mathbf{q}^c \mathbf{q}^c \mathbf{q}^c}^{\alpha_1 \alpha_2 \alpha_3 \alpha_4}, & V_{\mathbf{q}^c \mathbf{q}^c \mathbf{q}^s \mathbf{q}^s}^{\alpha_1 \alpha_2 \alpha_3 \alpha_4}.
\end{array} \quad (43)
$$

Therefore, in the most general case, multiple irreducible derivatives must be simultaneously considered even in the LID approach, though in many cases a single irreducible derivative can be probed.

Now we consider LID in the case where there are perturbative derivatives, and we focus on the common scenario of PD_1 (i.e., Hellman-Feynman forces). We can now reexamine the previous two examples. In the case of the complex derivative $d_{\bar{\mathbf{q}}\mathbf{q}}^{\alpha_1 \alpha_2}$, both the real and imaginary parts can be simultaneously measured, given that a derivative along $u_{\mathbf{q}^c}^{\alpha_2}$ will generate $V_{\mathbf{q}^c \mathbf{q}^c}^{\alpha_1 \alpha_2}$ and $V_{\mathbf{q}^s \mathbf{q}^c}^{\alpha_1 \alpha_2}$, in addition to $V_{\mathbf{q}^c \mathbf{q}^c}^{\alpha_2 \alpha_2}$ and $V_{\mathbf{q}^s \mathbf{q}^c}^{\alpha_2 \alpha_2}$. Therefore, even though our intent was to measure a single irreducible derivative, we immediately obtain a second one given that we have repeating irreducible representations in this example. In the simpler case of $d_{\bar{\mathbf{q}}\mathbf{q}}^{\alpha \alpha}$, PD_1 has precisely the same cost as PD_0 given that both cases require one measurement (assuming the undistorted energy is known); though PD_1 has the possibility of performing forward finite difference which would save a factor of two.

For the case of $d_{\bar{\mathbf{q}} \bar{\mathbf{q}} \mathbf{q} \mathbf{q}}^{\alpha_1 \alpha_2 \alpha_3 \alpha_4}$ using PD_1, all six real-q derivatives can be obtained from three measurements of the $\mathcal{N}' = 3$ derivatives of the forces: $\{u_{\mathbf{q}^c}^{\alpha_2}, u_{\mathbf{q}^c}^{\alpha_3}, u_{\mathbf{q}^c}^{\alpha_4}\}$, $\{u_{\mathbf{q}^c}^{\alpha_2}, u_{\mathbf{q}^c}^{\alpha_3}, u_{\mathbf{q}^s}^{\alpha_4}\}$, and

$\{u_{\mathbf{q}^c}^{\alpha_2}, u_{\mathbf{q}^3}^{\alpha_3}, u_{\mathbf{q}^4}^{\alpha_4}\}$. Therefore PD$_1$ will save a factor of two in this case.

We executed the LID approach using PD$_1$ for graphene at $\mathcal{N} = 2, 3, 4,$ and 5, with FTG up to $\tilde{\hat{\mathbf{S}}}_{\text{BZ}} = 12\hat{\mathbf{1}}, 2\hat{\mathbf{S}}_K, 2\hat{\mathbf{1}},$ and $2\hat{\mathbf{1}}$, respectively. In Fig. 4, we provide an example for $\mathcal{N} = 3, 4,$ and 5, where each data point corresponds to a single evaluation of $V_{u_1...u_{\mathcal{N}'}}^{u'_1}(\Delta)$ (i.e. up to $2^{\mathcal{N}'}$ DFT calculations for a given Δ). The red line is a quadratic fit to a subset of the points, as described in Sec. III C, and the intercept of this curve is the value of the indicated derivative. The values of all irreducible derivatives for $\hat{\mathbf{S}}_{\text{BZ}} = \hat{\mathbf{S}}_K$ at $\mathcal{N} = 2$ and $\mathcal{N} = 3$ are given in Table I, while the values for $3\hat{\mathbf{1}}$ and $\hat{\mathbf{S}}_{2K}$ at $\mathcal{N} = 3$ are given in Ref. [15] in Table SIII.

E. Maximally exploiting perturbative derivatives: bundled irreducible derivative approach

Here we consider the most efficient approach for extracting order $\mathcal{N}$ derivatives given PD$_\eta$, where $\eta < \mathcal{N}$, while restricting all calculations to the BvK supercell $\hat{\mathbf{S}}_{\text{BZ}}$; and this latter constraint will be removed in the next section. The intent is to determine as many irreducible derivatives as possible in a given measurement, and therefore we refer to this approach as bundled irreducible derivative (BID) approach; and given the use of the BvK supercell, we refer to this as the single-supercell bundled irreducible derivative (SS-BID) approach. In any BID approach, a basis is explicitly chosen to maximally avoid the block diagonal structure of the dynamical tensor. For simplicity, we focus on the most common case where only forces are *a priori* known, PD$_1$, though generalizing to other cases is straightforward. We have already defined the total number of unknowns which must be computed in the BvK supercell $\hat{\mathbf{S}}_{\text{BZ}}$ as $n_{ir}^{\hat{\mathbf{S}}_{\text{BZ}}}$. We now must determine the total number of measurements, denoted $n_m^{\hat{\mathbf{S}}_{\text{BZ}}}$, in some specifically chosen basis which is yet to be determined. It is straightforward to *a priori* determine the upper bound of $n_m^{\hat{\mathbf{S}}_{\text{BZ}}}$ using group theory alone for $\mathcal{N} = 2$.

$$n_m^{\hat{\mathbf{S}}_{\text{BZ}}} \leqslant \max_{\mathbf{q} \in \tilde{q}_{\text{BZ}}, \alpha \in \mathcal{U}_{\mathbf{q}}} \left\lceil \frac{a_{\mathbf{q}}^{\alpha}}{|\tilde{s}_q|} \right\rceil, \quad (44)$$

where $a_{\mathbf{q}}^{\alpha}$ is the number of times the α irreducible representation repeats at $\mathbf{q}$, and the outer bracket denotes the ceiling function. For a detailed example illustrating this procedure at second order in ZrO$_2$, see Appendix B.

Beyond second order, it is not straightforward to find the upper bound, but it is straightforward to determine the lower bound at arbitrary $\mathcal{N}$ using a counting argument:

$$n_m^{\hat{\mathbf{S}}_{\text{BZ}}} \geqslant \left\lceil \frac{n_{ir}^{\hat{\mathbf{S}}_{\text{BZ}}}}{(n_q n_a n_p - d)} \right\rceil, \quad (45)$$

where the numerator is the number of irreducible derivatives and the denominator is the number of nonzero force equations $n_F^{\hat{\mathbf{S}}_{\text{BZ}}} = n_q n_a n_p - d$. The exact $n_m^{\hat{\mathbf{S}}_{\text{BZ}}}$ can straightforwardly be determined by explicit calculation.

Having determined the bound of $n_m^{\hat{\mathbf{S}}_{\text{BZ}}}$, the specific choice of basis, which we call the "bundled basis," must be constructed for all measurements; being a set of real displacement vectors $\{b_1^i, \ldots, b_{\mathcal{N}-1}^i\}$, where $i = 1, \ldots, n_m^{\hat{\mathbf{S}}_{\text{BZ}}}$. It is useful to

store the $(n_q n_a n_p - d)n_m^{\hat{\mathbf{S}}_{\text{BZ}}}$ measured derivatives stacked into a vector $\mathbf{V}_b^{\hat{\mathbf{S}}_{\text{BZ}}}$, and all $n_{ir}^{\hat{\mathbf{S}}_{\text{BZ}}}$ irreducible derivatives which are contained within $\hat{\mathbf{S}}_{\text{BZ}}$ are stored in the vector $\mathbf{d}_{ir}^{\hat{\mathbf{S}}_{\text{BZ}}}$. The order $(\mathcal{N} - 1)$ chain rule generates a linear system of equations which relates the derivatives in the bundled basis $\mathbf{V}_b^{\hat{\mathbf{S}}_{\text{BZ}}}$ to the irreducible basis $\mathbf{d}_{ir}^{\hat{\mathbf{S}}_{\text{BZ}}}$: $\mathbf{V}_b^{\hat{\mathbf{S}}_{\text{BZ}}} = \hat{\mathbf{C}}^{\hat{\mathbf{S}}_{\text{BZ}}} \mathbf{d}_{ir}^{\hat{\mathbf{S}}_{\text{BZ}}}$; where $\hat{\mathbf{C}}^{\hat{\mathbf{S}}_{\text{BZ}}}$ is the $(n_q n_a n_p - d)n_m^{\hat{\mathbf{S}}_{\text{BZ}}} \times n_{ir}^{\hat{\mathbf{S}}_{\text{BZ}}}$ complex chain rule matrix. A necessary condition for the bundled basis is that rank($\hat{\mathbf{C}}^{\hat{\mathbf{S}}_{\text{BZ}}}$) = $n_{ir}^{\hat{\mathbf{S}}_{\text{BZ}}}$. The choice of bundled basis is not unique, but an obvious criterion is to minimize the condition number of $\hat{\mathbf{C}}^{\hat{\mathbf{S}}_{\text{BZ}}}$, which will ensure a minimal propagation of error upon solving for $\mathbf{d}_{ir}^{\hat{\mathbf{S}}_{\text{BZ}}}$. We explored this possibility by generating thousands of random bundled basis sets and choosing the one with the smallest condition number. We refer to this as the condition number optimized (CNO) bundled basis. The only downside to this is that it is inconvenient to disseminate the choices that we made.

A simple option is to create a sequence of rational numbers using the FTG's of a one dimensional lattice:

$$j = \bigcup_{n=1}^{\infty} \tilde{q}_n = \left\{ 0, \frac{1}{2}, \frac{1}{3}, \frac{2}{3}, \frac{1}{4}, \frac{3}{4}, \frac{1}{5}, \frac{2}{5}, \frac{3}{5}, \frac{4}{5}, \cdots \right\}, \quad (46)$$

where $\tilde{q}_n$ corresponds to q points in one dimensional supercell n. The first bundled vector is obtained by iterating over every displacement within $\hat{\mathbf{S}}_{\text{BZ}}$ and imparting an amplitude of $\cos(2\pi j_n n)$, where j_n is the nth element of the set j and n has an inner loop running over the n_p displacements and an outer loop running over all $n_a n_q$ atoms in $\hat{\mathbf{S}}_{\text{BZ}}$. The remaining bundled basis vectors are generated by continuing along the sequence j. We refer to this as the simple bundled basis (SBB), and in all cases we tested the vectors generated in this manner did fulfill rank($\hat{\mathbf{C}}^{\hat{\mathbf{S}}_{\text{BZ}}}$) = $n_{ir}^{\hat{\mathbf{S}}_{\text{BZ}}}$. While the condition number of the resulting $\hat{\mathbf{C}}^{\hat{\mathbf{S}}_{\text{BZ}}}$ for SBB will generally be larger than the CNO basis, the differences in the resulting irreducible derivatives were typically very small (direct comparisons are made in Ref. [15], Fig. S3). All BID results in this paper were generated using the SBB basis unless otherwise noted.

We illustrate some specific results using BID in Fig. 4, indicated by a dashed line. As shown, the results agree with the LID approach to within fractions of a percent. This excellent agreement signifies that we successfully resolved the quadratic error tails within the SBB bundled basis, indicating that the Hellman-Feynman forces were *maximally* harnessed without any appreciable loss in precision.

Given that our method works purely in terms of irreducible derivatives, we are guaranteed to satisfy all possible symmetries of the order $\mathcal{N}$ Taylor series by construction; and our BID approach allows them to be extracted in the smallest number of measurements. Therefore, it is useful to compare with competing approaches which implement symmetry using extrinsic real-space symmetry approaches, and we focus on the example of the rock salt structure at $\mathcal{N} = 3$.

A recent paper compared the efficiency of three popular approaches to compute cubic terms using finite displacements [85], which we shall label by the codes which implement them: AAPL [85], PHONO3PY [93], and SHENGBTE [84].
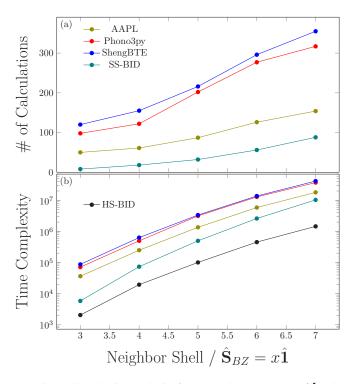
FIG. 5. Complexity analysis for rocksalt structure at $\mathcal{N} = 3$, comparing existing published methods (SHENGBTE, PHONO3PY, and AAPL, taken from Ref. [85]) with our approaches (SS-BID and HS-BID); including (a) number of required DFT calculations and (b) time complexity assuming that the DFT calculations scale quadratically with system size [21,22]. Existing methods only calculate the derivatives out to the x neighbor shell (where x is the horizontal axis) within supercell $\hat{\mathbf{S}}_{BZ} = x\hat{\mathbf{1}}$, while our methods computes *all* derivatives within the corresponding supercell.

Figure 5(a) replots the results that were presented in Ref. [85], which determines the number of DFT calculations required to determine all cubic derivatives within some real-space cutoff shell within a given supercell, and serves as a measure of the extent to which symmetry has been accounted for. We have reproduced the results for the case of PHONO3PY, which ensures we have properly understood the conventions and assumptions when using PHONO3PY in Ref. [85]; and we assume that the analogous procedures were applied for AAPL and SHENGBTE, as we did not attempt to interpret the choices made in executing these latter codes.

It is important to first clarify the x axis of Fig. 5(a), which we labeled as being both the "Neighbor Shell" and $\hat{\mathbf{S}}_{BZ} = x\hat{\mathbf{1}}$. For the competing approaches (i.e., AAPL, PHONO3PY, and SHENGBTE), this means that a $\hat{\mathbf{S}}_{BZ} = x\hat{\mathbf{1}}$ supercell is constructed and only derivatives within a x-neighbor shell are retained. Alternatively, when we used our SS-BID method for comparison, we compute *all possible derivatives* which exist within $\hat{\mathbf{S}}_{BZ} = x\hat{\mathbf{1}}$. Therefore this is not a fair comparison with respect to our space group irreducible approach. It is worth noting that if one does not include a real-space truncation in the PHONO3PY code, allowing it to compute all derivatives within the supercell, the numbers are substantially larger. For example, if one execute $\hat{\mathbf{S}}_{BZ} = 3\hat{\mathbf{1}}$ in PHONO3PY without any truncation, the number of DFT runs increases to 194; nearly

doubling as compared to the truncated case [i.e., $x = 3$ in Fig. 5(a)].

Figure 5(a) shows that AAPL, PHONO3PY, and SHENGBTE all overestimate the actual number of calculations which are required to extract *all* irreducible derivatives within the supercell. To give an idea of the computational speedup, we assume that the first-principles method will scale as the square of the number of atoms [21,22], and plot the total time in Fig. 5(b), demonstrating a substantial gain over all competing approaches.

In order to clearly demonstrate the group theoretical nature of our results, we explicitly list all irreducible derivatives for the case of $\hat{\mathbf{S}}_{BZ} = 2\hat{\mathbf{1}}$ in Appendix A. As shown, there are 33 real irreducible derivatives and these can all be obtained within a single measurement according explicit calculation. We emphasize that the result of our group theoretical analysis is not original in this case, as Birman *et al.* first derived all possible results for a third-order product, symmetric or otherwise, in $Fm\bar{3}m$ [94].

F. Bundled irreducible derivatives with hierarchical supercells

Here we consider an alternative BID approach which demands that each irreducible derivative is computed within the smallest possible supercell in which it fits; and we refer to this as the hierarchical supercell bundled irreducible derivative (HS-BID) approach. Our minimum supercell multiplicity equation dictates that for three dimensional materials having uniform supercells, the BvK supercell can be completely avoided for $\mathcal{N} \leqslant 3$, and therefore HS-BID will yield a substantial increase in computational efficiency for first-principles approaches which scale in a super-linear fashion, as most do, despite the fact that more total calculations are required.

The first step is to categorize the smallest supercell into which each irreducible derivatives fits. Therefore, for all $\tilde{\mathcal{S}} \in \tilde{\mathcal{S}}_{BZ}$, we must determine the smallest supercell $\hat{\mathbf{S}}_{\tilde{\mathcal{S}}}$ which contains at least one $Q \in \tilde{\mathcal{S}}$; and the set of all supercells is denoted as $\tilde{\mathbf{S}}_{BZ}$, where $|\tilde{\mathbf{S}}_{BZ}| \leqslant |\tilde{Q}_{IBZ}|$. Additionally, we construct a set $\tilde{\mathcal{S}}_{\hat{\mathbf{S}}}$ which contains the set of all $\tilde{\mathcal{S}}_Q$ commensurate with $\hat{\mathbf{S}}$. Furthermore, for every $\tilde{\mathcal{S}}_{\hat{\mathbf{S}}}$, we create a subset denoted $\tilde{\mathcal{S}}_{\hat{\mathbf{S}}}^{\vee}$, which consists of all orbits $\tilde{\mathcal{S}}_Q$ that are contained by $\hat{\mathbf{S}}$ and *not* contained by any $\hat{\mathbf{S}}_j$ where $|\det(\hat{\mathbf{S}}_j)| < |\det(\hat{\mathbf{S}})|$. Now, the number of irreducible derivatives which must be computed in a given supercell is $n_{ir}^{\vee\hat{\mathbf{S}}} = \sum_{\tilde{\mathcal{S}} \in \tilde{\mathcal{S}}_{\hat{\mathbf{S}}}^{\vee}} n_{ir}^{\tilde{\mathcal{S}}}$. We will also define corresponding quantities $\tilde{\mathcal{S}}_{\hat{\mathbf{S}}}^{\wedge}$ and $n_{ir}^{\wedge\hat{\mathbf{S}}}$ to characterize the irreducible derivatives in $\hat{\mathbf{S}}$ which are contained in a smaller supercell; where $n_{ir}^{\hat{\mathbf{S}}} = n_{ir}^{\vee\hat{\mathbf{S}}} + n_{ir}^{\wedge\hat{\mathbf{S}}}$.

In order to illustrate the definitions in the preceding paragraph, we consider graphene at $\mathcal{N} = 3$ and $\hat{\mathbf{S}}_{BZ} = 3\hat{\mathbf{1}}$, where

$$\tilde{Q}_{IBZ} = \{[\Gamma, \Gamma, \Gamma], [\Gamma, \bar{K}, K], [K, K, K], [\Gamma, \Delta_0, \Delta_3],$$
$$[\Delta_0, \Delta_0, \Delta_0], [K, \Delta_0, \Delta_5], [\Delta_0, \Delta_2, \Delta_4]\}, \quad (47)$$

with the notation taken from Fig. 1(b). The set of supercells $\tilde{\mathbf{S}}_{BZ}$ is

$$\tilde{\mathbf{S}}_{BZ} = \{\hat{\mathbf{1}}, \hat{\mathbf{S}}_K, 2\hat{\mathbf{1}} + \hat{\sigma}_x, 3\hat{\mathbf{1}}\}. \quad (48)$$

Finally, the $\tilde{\mathcal{S}}_{\hat{\mathbf{S}}}^{\vee}$ for each $\hat{\mathbf{S}} \in \tilde{\mathbf{S}}_{\text{BZ}}$ is

$$
\begin{aligned}
\tilde{\mathcal{S}}_{\hat{\mathbf{1}}}^{\vee} &= \{[\Gamma, \Gamma, \Gamma]\} \quad \tilde{\mathcal{S}}_{\hat{\mathbf{S}}_K}^{\vee} = \{[K, K, K], [\Gamma, \bar{K}, K]\}; \\
\tilde{\mathcal{S}}_{2\hat{\mathbf{1}}+\hat{\sigma}_x}^{\vee} &= \{[\Delta_0, \Delta_0, \Delta_0], [\Gamma, \Delta_0, \Delta_3]\}; \\
\tilde{\mathcal{S}}_{3\hat{\mathbf{1}}}^{\vee} &= \{[K, \Delta_0, \Delta_5], [\Delta_0, \Delta_2, \Delta_4]\}.
\end{aligned}
\tag{49}
$$

Here we see that only two out of the seven total Q need to be computed in the BvK supercell; though it should be noted that those two have the lowest symmetry.

The next step is to determine the bundled basis for each $\hat{\mathbf{S}} \in \tilde{\mathbf{S}}_{\text{BZ}}$. Therefore we split $\mathbf{d}_{ir}^{\hat{\mathbf{S}}}$ into two separate vectors $\mathbf{d}_{\vee}^{\hat{\mathbf{S}}}$ and $\mathbf{d}_{\wedge}^{\hat{\mathbf{S}}}$ containing the irreducible derivatives which do not ($\vee$) and do ($\wedge$) fit into a smaller supercell, respectively. Similarly, the previously defined chain rule matrix $\hat{\mathbf{C}}^{\hat{\mathbf{S}}}$ can be split into two respective pieces $\hat{\mathbf{C}}_{\vee}^{\hat{\mathbf{S}}}$ and $\hat{\mathbf{C}}_{\wedge}^{\hat{\mathbf{S}}}$. Finally, we can obtain the unknown derivatives which only fit in $\hat{\mathbf{S}}$: $\mathbf{d}_{\vee}^{\hat{\mathbf{S}}} = (\hat{\mathbf{C}}_{\vee}^{\hat{\mathbf{S}}})^+ (\mathbf{V}_b^{\hat{\mathbf{S}}} - \mathbf{C}_{\wedge}^{\hat{\mathbf{S}}} \mathbf{d}_{\wedge}^{\hat{\mathbf{S}}})$, where $(\hat{\mathbf{C}}_{\vee}^{\hat{\mathbf{S}}})^+$ refers to the pseudoinverse. A necessary condition for the bundled basis is that $\text{rank}(\hat{\mathbf{C}}_{\vee}^{\hat{\mathbf{S}}}) = n_{ir}^{\vee\hat{\mathbf{S}}}$, and the basis can be chosen using the same schemes as described for SS-BID. Once the bundled basis has been chosen for each $\hat{\mathbf{S}} \in \tilde{\mathbf{S}}_{\text{BZ}}$, the CFD measurements can be performed, and then the irreducible derivatives can be extracted from the smallest to largest supercell. It should be noted that all calculations can be performed simultaneously, given that the bundled basis can be determined *a priori*.

The only remaining idea to be introduced is the notion of "overbundling" irreducible derivatives. Given that $n_{ir}^{\vee\hat{\mathbf{S}}}/n_F^{\hat{\mathbf{S}}}$ is typically not a round number, it may be possible to obtain irreducible derivatives which fit in a smaller supercell for free. Specifically, derivatives tallied in $n_{ir}^{\wedge\hat{\mathbf{S}}}$ may possibly be added without any increase in $n_m^{\hat{\mathbf{S}}}$; though in general the bundled basis will need to be modified to properly sample the additional derivatives.

It is useful to compare the performance of HS-BID with SS-BID, in addition to the competing approaches [see Fig. 5(b)]. Assuming the first-principles method scales quadratically with system size, HS-BID is more than an order of magnitude faster than all competing approaches that we examined. The speedup would be far more dramatic for first-principles methods with poorer scaling, such as hybrid functionals. It should be emphasized that the speedup of HS-BID compared to SS-BID will be far more dramatic for $\mathcal{N} = 2$ as compared to $\mathcal{N} = 3$, treated in this example. Given the efficiency of our new methods, crystals with increasingly complex unit cells may be treated using DFT, and methods which scale poorly (e.g., hybrid functionals) may now be used to compute phonons and their interactions more regularly.

Finally, we discuss factors related to the quality of the measurements. Given that some measurements may be deficient (i.e., poor quadratic error tails), it may be easier to simply dispense with them as opposed to fixing them. For example, if one is not overbundling, there may be room to simply remove a derivative while keeping the chain rule matrix full rank; and we refer to this as "pruning." If not, one can simply add additional measurements, which we refer to as "overmeasuring," and then one can prune away the problem derivatives.

IV. ASSESSING THE RESULTS

A. General considerations

No matter what formalism is used to compute the Taylor series of the Born-Oppenheimer surface, one needs some clear criteria to assess the quality of the results. Many studies predict some observable and then compare to experiment. This is not an ideal test on its own, even if successful, because it easily allows for a cancellation of errors and human bias to interact in a dangerous manner; especially so when an approach simultaneously fits many derivatives. Ideally, the test should be purely self-consistent, only answering how well the Born-Oppenheimer surface of the first-principles method at hand is captured. In this vein, some studies compare their results to first-principles molecular dynamics on small supercells. We note that first-principles molecular dynamics contains the Taylor series to infinite order, so failure will not differentiate between a poor expansion and activation of higher-order terms not included in the expansion being tested. Furthermore, one can only probe relatively small FTG's in this manner, due to the computational expense of first-principles approaches.

Here we consider several different validations for Taylor series, the first being completely generic to any method, and the others being specific to finite displacements. The first is the strain derivatives of the phonons, where the Nth-order strain derivative will result in an infinite range coupling of the $(N + 2)$th-order force tensor. This is an ideal test in that strain derivatives can efficiently be calculated by simply perturbing the lattice vectors in the context of a phonon calculation; which will not alter the number of atoms within the unit cell in any given calculation. A usual scenario is the first volume derivative of the phonons, which, in conjunction with the phonons, gives rise to the well-known Grüneisen parameters [1]. Furthermore, the Grüneisen parameters are directly connected to thermodynamic observables, and therefore properly resolving them is physically well justified; which is why Grüneisen parameters have often served as a test of cubic phonon interactions [82]. The other two tests we perform are more specific to finite displacement calculations: assessing the quality of the quadratic error tails and comparing results of BID and LID approaches. Below we illustrate all three tests.

B. Strain derivatives of the phonons

We begin by assessing the order N strain derivatives, and we restrict our attention identity strains (i.e., uniform in all directions) for simplicity. Taylor series expanding the dynamical tensor to first order for N selected $\mathbf{q}_i$, contracting with the corresponding acoustic displacement vectors to leading order in $\mathbf{q}$, taking the small $\mathbf{q}$ limit of the corresponding displacements, and taking the identity strain derivatives, we arrive at an analytic expression for the Nth-order identity strain derivative of the dynamical matrix. We have restricted ourselves to crystals which have no internal degrees of

freedom, resulting in the following equation:

$$\frac{\partial^N D_{\bar{\mathbf{q}}\mathbf{q}}^{mn}}{\partial \epsilon_A^N} = \frac{\sqrt{n_a^N}}{d^N} \sum_{\mathbf{t}} e^{-i2\pi\mathbf{q}\cdot\mathbf{t}} \sum_{\substack{\mathbf{t}_1 \ldots \mathbf{t}_N \\ b_1 \ldots b_N \\ \beta_1 \ldots \beta_N}} \Phi_{\mathbf{0},\,\mathbf{t},\,\mathbf{t}_1,\ \ \ldots,\mathbf{t}_N}^{m,n,(b_1,\beta_1),\ldots,(b_N,\beta_N)}$$

$$\times \sum_{\alpha_1 \ldots \alpha_N} \prod_{k=1}^{N} (\mathbf{t}_k\hat{\mathbf{a}} + \mathcal{A}_{b_k}) \cdot \mathbf{e}_{\alpha_k} \langle u_{\Gamma}^{(b_k,\beta_k)} | \psi_{\Gamma}^{\alpha_k} \rangle, \quad (50)$$

where ϵ_A is the unnormalized identity strain, $\mathbf{e}_i$ is a d-dimensional unit vector, and $|\psi_{\Gamma}^{\alpha}\rangle$ is an acoustic vector at the zone center. For crystals with internal degrees of freedom, or for arbitrary strain states, one must explicitly compute the first-order corrections to the $\mathbf{q}$ dependence of the acoustic modes; and this requires the phonons (for $N = 1$, see Refs. [95,96] for further details). The key point is that it is straightforward to directly measure the left-hand side of Eq. (50) by computing the phonons at a series of different uniform strains, resulting in a set of strain derivative of the phonons defined over some FTG which can then be Fourier interpolated. Additionally, the corresponding quantity can be predicted purely using the $\mathcal{N} = N + 2$ irreducible derivatives on the right-hand side of Eq. (50); and the factors $\mathbf{t}_k\hat{\mathbf{a}}$ mean that long-range terms in the force tensor will be amplified, creating a test that is sensitive to noise in long-range terms.

For the case of $N = 1$, the Grüneisen parameters may be constructed as

$$\gamma_{\mathbf{q}}^i = -\frac{1}{2}\left(\hat{\mathbf{U}}_{\mathbf{q}}^{\dagger}\hat{\mathbf{M}}^{\frac{1}{2}}\hat{\mathbf{D}}_{\bar{\mathbf{q}}\mathbf{q}}^{-1}\frac{\partial\hat{\mathbf{D}}_{\bar{\mathbf{q}}\mathbf{q}}}{\partial\epsilon_A}\hat{\mathbf{M}}^{-\frac{1}{2}}\hat{\mathbf{U}}_{\mathbf{q}}\right)_{ii}, \quad (51)$$

where $\hat{\mathbf{U}}_{\mathbf{q}}$ is the unitary transformation that diagonalizes $\hat{\mathbf{M}}^{-1/2}\hat{\mathbf{D}}_{\bar{\mathbf{q}}\mathbf{q}}\hat{\mathbf{M}}^{-1/2}$ and $\hat{\mathbf{M}}$ is the mass matrix. Equation (50) for $N = 1$ in conjunction with Eq. (51) is consistent with the equation presented in Ref. [96].

We begin by comparing our measured and predicted Grüneisen parameters in Fig. 6(a). The direct measurement of the Grüneisen parameters via strain central finite difference are denoted with circles (diamonds) for the in-plane (out-of-plane) modes, while the blue lines are obtained via Fourier interpolation; and these results are referred to as "Measured," given that they are numerically exact for the actual points. The results obtained from using the cubic dynamical tensor in conjunction with Eq. (50) are presented for several different FTG's. It should be noted that there are no data points on these curves, as no part of these curves are numerically exact. The FTG $\hat{\mathbf{S}}_{\mathrm{BZ}} = 2\hat{\mathbf{I}}$ displays relatively poor agreement overall, though the uppermost branch is in good agreement, and several other branches have a proper shape but are simply shifted ($\hat{\mathbf{S}}_{\mathrm{BZ}} = \hat{\mathbf{S}}_K$ displayed very similar results, and is not shown for clarity). This is consistent with the interpretation that the dynamical tensor is robust, but the FTG is simply too small. Moving to the next larger FTG, $\hat{\mathbf{S}}_{\mathrm{BZ}} = 3\hat{\mathbf{I}}$, the results markedly improve, with only relatively small disagreement; here the discrepancies are likely too large for sensitive quantities like thermal conductivity. The next larger FTG, $\hat{\mathbf{S}}_{\mathrm{BZ}} = 2\hat{\mathbf{S}}_K$, shows relatively good agreement, with only minor deviations. The $\mathcal{N} = 3$ irreducible derivatives for all cases are provided in Ref. [15] Table SIII; with
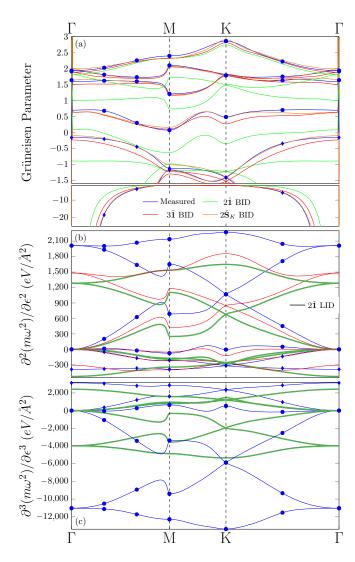

FIG. 6. (a) Grüneisen parameters of graphene directly measured using identity strain derivatives of the phonons and Fourier interpolation (blue points and lines; diamonds and circles correspond to out-of-plane and in-plane modes, respectively) and via Eq. (50), which uses the cubic irreducible derivatives at various mesh densities. (b) and (c) follow the same conventions, but for the second and third strain derivatives, respectively; and both panels display the LID results for $2\hat{\mathbf{I}}$ in gray, showing near perfect agreement with BID results.

$\hat{\mathbf{S}}_{\mathrm{BZ}} = 2\hat{\mathbf{S}}_K$ having 215 purely real or imaginary terms. All the preceding results were obtained using SS-BID, but the results using HS-BID and LID are extremely similar (see Ref. [15], Fig. S1).

The quartic elements of the dynamical tensor can be probed via the second strain derivatives of the phonons, which is shown Fig. 6(b); where the second strain derivative alone is plotted. For the coarsest FTG, $\hat{\mathbf{S}}_{\mathrm{BZ}} = 2\hat{\mathbf{I}}$, the general shape is smooth and resembles the numerically exact measurements, though the deviations are relatively large. However, the near perfect agreement of LID and BID suggests that the derivatives are robust, but a larger FTG is needed. Moving to the next larger FTG, $\hat{\mathbf{S}}_{\mathrm{BZ}} = 3\hat{\mathbf{I}}$, the results improve for the out-of-plane modes, while the in-plane mode results have shifted in the
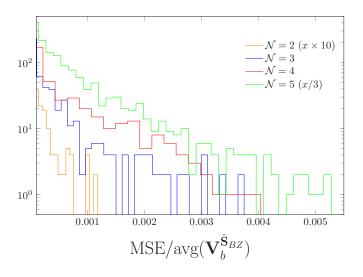
FIG. 7. A histogram of mean square error, associated with the quadratic fits to the central finite difference calculations as a function of Δ within the SBB in the SS-BID approach, *divided* by the average magnitude of the SS-BID SBB derivatives. Note that values for $\mathcal{N} = 2$ are multiplied by ten while the $\mathcal{N} = 5$ values are divided by three for ease of viewing. FTG's of $6\hat{\mathbf{1}}$, $2\hat{\mathbf{S}}_K$, $2\hat{\mathbf{1}}$, and $2\hat{\mathbf{1}}$, are used for $\mathcal{N} = 2$–5, respectively.

proper direction, but not substantially enough. Even larger FTG's would be needed for a higher resolution of the results, but we do not proceed further due to computational expense.

The quintic elements of the dynamical tensor can be probed via the third strain derivatives of the phonons, which is shown Fig. 6(c). In this case, only $\hat{\mathbf{S}}_{BZ} = 2\hat{\mathbf{1}}$ was attempted. Once again, LID and BID agree extremely well in this case, suggesting that the derivatives are robust. While the overall shape of the curves are reasonable, it is clear that a larger FTG would be required to resolve these third strain derivatives.

In summary, strain derivatives can be used as a critical test of the dynamical tensor, no matter what method is used to compute it. A more general equation can be derived for an arbitrary strain derivative, beyond the simple identity strain considered in Eq. (50), which would allow for a much more detailed test; as a larger fraction of the dynamical tensor would be probed. We leave this to future work. It also should be noted that the logic of using strain derivatives of phonons as a test could be inverted to instead use them as a rich source of information which could be used to assist in extracting the dynamical tensor, and there are several studies which have begun to pursue this [52,97].

C. Assessing quadratic error tails

If central finite difference is being used to measure derivatives, then it is critical to assess the quality of the quadratic error tails. Our algorithm for choosing the set of Δ used to construct the quadratic error tail is detailed in Sec. III C. Once the Δ are selected and a least squares fit is performed, there will be a mean square error associated with each quadratic error tail, and a histogram can be constructed (see Fig. 7). The results are as expected, with the error increasing as $\mathcal{N}$ increases from two to five. Furthermore, this should be performed as a diagnostic analysis, and the first evaluation of this
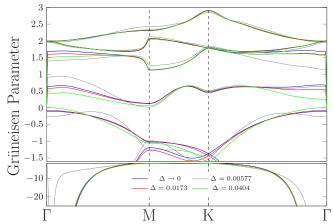

FIG. 8. Comparison of the Grüneisen parameters in graphene obtained from cubic irreducible derivatives within $\hat{\mathbf{S}}_{BZ} = 2\hat{\mathbf{S}}_K$ using SS-BID. The blue curve uses our algorithm outlined in Sec. III C to properly extrapolate Δ to zero, while the other curves simply use a single value of Δ.

data did indeed reveal numerous problematic derivatives. The offending derivatives can be inspected to resolve any issues, which usually involves adding additional Δ, increasing the convergence parameters of the DFT calculations, or simply pruning the offending derivative (see Sec. III F).

Given the common practice of using a single Δ to estimate the value of a derivative, as opposed to properly extrapolating to $\Delta \rightarrow 0$, it is interesting to test the efficacy of this on the predicted Grüneisen parameters for graphene with $\hat{\mathbf{S}}_{BZ} = 2\hat{\mathbf{S}}_K$ (see Fig. 8). As shown, substantial errors occur if Δ is too large or too small, though reasonable results can be obtained with a properly chosen single Δ in this case; but it can be difficult to choose *a priori*. We have observed that the results become more sensitive to a single Δ as $\hat{\mathbf{S}}_{BZ}$ increases (not shown), most likely because more irreducible derivatives are being simultaneously measured. For a sufficiently large FTG, it is possible that no single Δ will be effective.

D. Bundled versus Lone derivatives

Another obvious test is to compare BID to LID. Of course, if extremely high reliability and precision is needed, and one has the computing resources to execute LID, then LID is the best route. However, this will not always be possible, and BID will frequently be needed. Bundled derivatives are challenging in the sense that the many irreducible derivatives that are simultaneously being measured may have starkly different quadratic error tails, which may result in a relatively small region of Δ which is resolvable as quadratic (see Ref. [15], Fig. S2a, for a problematic example). As a result, very stringent convergence parameters within DFT may be required to successfully resolve this quadratic region. Alternatively, LID measures as few irreducible derivatives as possible, and the error tails tend to be much better behaved in this method. Therefore, when using BID, one can still compute some fraction of irreducible derivatives using LID as a test; perhaps either a subgroup of the given FTG, or maybe some random selection. Figure 9 provides a comparison between
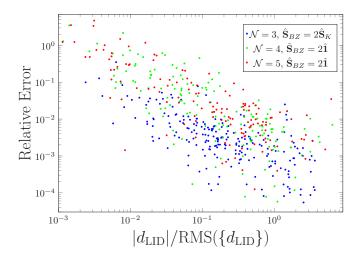
FIG. 9. A plot comparing the irreducible derivatives computed using LID and SS-BID. The x axis denotes relative magnitude ($|d_{\mathrm{LID}}|/\mathrm{RMS}(\{d_{\mathrm{LID}}\})$) and the y axis denotes relative error ($|d_{\mathrm{LID}} - d_{\mathrm{BID}}|/|d_{\mathrm{LID}}|$). For $\mathcal{N} = 3$ and 4, all irreducible derivatives are sampled, while only a subset is provided for $\mathcal{N} = 5$.

the irreducible derivatives as computed using LID and BID for $\mathcal{N} = 3$–5. As expected, the error is smallest for $\mathcal{N} = 3$, and increases for $\mathcal{N} = 4$ and 5. The terms that have relatively large errors tend to be sufficiently small in magnitude relative to the average magnitude.

V. SUMMARY AND CONCLUSIONS

We have presented a general framework for characterizing and computing phonons and their interactions. The first aspect of our work is to write the Taylor series expansion of the Born-Oppenheimer surface purely in terms of space group irreducible derivatives. Space group irreducible derivatives guarantee invariance to all space group operations, homogeneity of free space, and permutation symmetry with respect to the order of differentiation; resulting in a Taylor series that satisfies all the possible symmetries *by construction*.

We demonstrate that it should not be assumed that numerical implementations of extrinsic symmetry approaches are capturing all symmetry (see Secs. III E and III F, for examples), and such approaches may produce potentials with broken symmetry that are susceptible to all sorts of uncontrolled errors. Space group irreducible derivatives not only guarantee that all symmetry is satisfied by construction, but they also provide a convenient means for storing and disseminating results; and this will be critical to data based approaches to the physics of materials.

The second contribution of this work was to resolve an apparently outstanding mathematical problem regarding the translation group. In particular, we resolve the minimum supercell problem, which is to find the smallest possible supercell that will accommodate $\mathcal{N}$ wave vectors in a d dimensional crystal. We show that this problem is equivalent to constructing the modulo L kernel space of the integer matrix $\hat{\mathcal{Q}}'$ under consideration (obtained by multiplying $\hat{\mathcal{Q}}$ by L and removing any one row); which we prove can be

achieved using the Smith normal form, resulting in the MSM equation [Eq. (36)]. In practice, this approach can always be executed with negligible computational cost. Furthermore, the MSM equation dictates that for any FTG of an arbitrary d-dimensional crystal at $\mathcal{N} = 2$ (i.e. phonons), in addition to any FTG's corresponding to $\hat{\mathbf{S}}_{\mathrm{BZ}} = n\hat{\mathbf{1}}$ at arbitrary order $\mathcal{N}$, the largest necessary supercell multiplicity is $L_m^{\min(\mathcal{N}-1,d)}$. The implication for $\mathcal{N} = 2$ and $d \leqslant 3$ was only recently realized [76], while the same cannot be said for $\mathcal{N} = d = 3$; which will have a major impact for the computation of cubic interactions using finite displacement approaches.

The third contribution of this work is the formulation of two finite displacement approaches for computing phonons and their interactions. First, we formulate the lone irreducible derivative (LID) approach, which measures a single irreducible derivative, or as few as possible, at a time in the smallest possible supercell. The LID approach is the generalization of the original frozen phonon approach to fully exploit intrinsic symmetrization and minimum supercells at an arbitrary order. While LID does not efficiently exploit perturbative derivatives, it should be the method of choice when the most precise results are needed for a finite difference calculation of a given irreducible derivative. The second finite displacement approach we develop is the bundled irreducible derivative (BID) approach; which maximally exploits perturbative derivatives in order to obtain higher derivatives via finite difference. BID guarantees that all derivatives are extracted in the smallest possible number of calculations. We demonstrate how to implement this BID approach both using a single supercell approach, and using a hierarchical supercell approach, which guarantees that all derivatives are executed in the smallest supercell possible.

We explicitly execute both LID and BID using the Hellman-Feynman forces (i.e., first derivatives) for graphene; computing irreducible derivatives at $\mathcal{N} = 2$–5. We explicitly tabulate all irreducible derivatives for $\hat{\mathbf{S}}_{\mathrm{BZ}} = 2\hat{\mathbf{S}}_K$ at $\mathcal{N} = 3$; which amounts to 215 purely real or imaginary numbers. We note that $\hat{\mathbf{S}}_{\mathrm{BZ}} = 2\hat{\mathbf{S}}_K$ will reproduce the numerically exact Grüneisen parameters with a relatively high fidelity. For cubic interactions in the rock salt structure, we have demonstrated that our hierarchical supercell bundled irreducible derivative (HS-BID) is more than an order of magnitude faster than approaches implemented in the SHENGBTE, PHONO3PY, and AAPL codes. Corresponding speedups at second order will be even more dramatic.

While perturbation theory should be used to the highest-order possible whenever possible, the many scenarios where it is not yet available, which range from practical issues in some particular DFT code or difficult technical issues associated with beyond DFT methods, imply that finite difference will play a critical role in the foreseeable future. Our developments will allow finite displacement based methods to be implemented as efficiently as possible. Finally, we emphasize that techniques which use a first-principles molecular dynamics trajectory as data to fit phonon interactions can also exploit our hierarchical supercell approach.

Our final development relates to assessing the quality of phonon interactions. We build upon the tradition of using the Grüneisen parameters as a test of cubic phonon interactions. We derive an analytic equation to compute the Nth uniform

strain derivative of the phonons, which is a linear combination of the $(N+2)$th irreducible derivatives. The strain derivatives of the phonons are straightforward to compute, and provide a stringent, infinite ranged test of the force tensor, which is constructed from the irreducible derivatives.

The above developments should greatly assist in advancing the computation of phonons and their interactions, which will impact a broad range of applications. An important point that has not been addressed in this paper is that object oriented, modular software has been developed to implement all of the ideas in this paper at arbitrary order $\mathcal{N}$. This free, open source software will be disseminated shortly, and described in the appropriate forum.

APPENDIX A: APPLICATIONS TO THE ROCKSALT STRUCTURE

In this Appendix, we consider the rock salt structure and present all space group irreducible derivatives for $\mathcal{N}=3$ in the supercell $\hat{\mathbf{S}}_{\mathrm{BZ}} = 2\hat{\mathbf{1}}$. The rocksalt structure has space group $Fm\bar{3}m$, and the structure can be defined as

$$\hat{\mathbf{a}} = \frac{a}{2}\begin{bmatrix} 0 & 1 & 1 \\ 1 & 0 & 1 \\ 1 & 1 & 0 \end{bmatrix}, \quad \begin{aligned} \mathbf{A}_1 &= (0,0,0), \\ \mathbf{A}_2 &= \frac{a}{2}(1,1,1), \end{aligned} \quad \text{(A1)}$$

where a is the lattice constant. Given the FTG $\hat{\mathbf{S}}_{\mathrm{BZ}} = 2\hat{\mathbf{1}}$, we have

$$\tilde{q}_{\mathrm{BZ}} = \{\Gamma, L_a, L_b, L_c, L_d, X_x, X_y, X_z\}, \quad \text{(A2)}$$

$$\tilde{q}_{\mathrm{IBZ}} = \{\Gamma, L_a, X_x\}, \quad \text{(A3)}$$

where

$$\begin{aligned} \Gamma &= (0,0,0), \quad L_a = \left(\tfrac{1}{2},0,0\right), \quad L_b = \left(0,\tfrac{1}{2},0\right), \\ L_c &= \left(0,0,\tfrac{1}{2}\right), \quad L_d = \left(\tfrac{1}{2},\tfrac{1}{2},\tfrac{1}{2}\right), \quad X_x = \left(0,\tfrac{1}{2},\tfrac{1}{2}\right), \\ X_y &= \left(\tfrac{1}{2},0,\tfrac{1}{2}\right), \quad X_z = \left(\tfrac{1}{2},\tfrac{1}{2},0\right). \end{aligned} \quad \text{(A4)}$$

The next step is to symmetrize the displacements at each $\mathbf{q} \in \tilde{q}_{\mathrm{IBZ}}$, where $\tilde{G}_\Gamma = O_h$, $\tilde{G}_L = D_{3d}$, and $\tilde{G}_X = D_{4h}$. Decomposing each representation in terms of irreducible representations (and removing the acoustic modes), we have

$$\begin{aligned} \hat{\mathcal{U}}_\Gamma &= T_{1u}, \\ \hat{\mathcal{U}}_{L_i} &= A_{1g} \oplus E_g \oplus A_{1u} \oplus E_u, \\ \hat{\mathcal{U}}_{X_i} &= 2A_{2u} \oplus 2E_u. \end{aligned} \quad \text{(A5)}$$

The induced representations of each $u_{\mathbf{q}}^\alpha$ must be constructed:

u_L^α	A_{1g}	E_g	A_{2u}	E_u
$u_{\tilde{s}_L}^{\alpha_k}$	A_{1g}	E_g	A_{2u}	E_u
	T_{2g}	T_{2g}	T_{1u}	T_{1u}
		T_{1g}		T_{2u}

u_X^α	A_{2u}	E_u
$u_{\tilde{s}_X}^{\alpha_k}$	T_{1u}	T_{1u}
		T_{2u}

$$\text{(A6)}$$

where the induced representations are listed directly below each $u_{\mathbf{q}}^\alpha$, the index k enumerates them, and α_k is an irreducible representation of O_h. For the Γ point, $u_\Gamma^\alpha = u_{\tilde{s}_\Gamma}^\alpha$. We now have all the information we need to deduce if a star product can be nonzero.

For $\mathcal{N}=3$, the irreducible Q must be constructed:

$$\begin{aligned} \tilde{Q}_{\mathrm{IBZ}} = \{&[\Gamma,\Gamma,\Gamma], [\Gamma,L_a,L_a], [L_a,L_b,X_z], \\ &[\Gamma,X_z,X_z], [X_x,X_y,X_z]\}. \end{aligned} \quad \text{(A7)}$$

Next, each $Q \in \tilde{Q}_{\mathrm{IBZ}}$ must be examined. For $[\Gamma,\Gamma,\Gamma]$, there are only T_{1u} vectors, and the symmetric direct product can be constructed (brackets denote symmetric product)

$$[T_{1u} \otimes T_{1u} \otimes T_{1u}] = A_{2u} \oplus 2T_{1u} \oplus T_{2u}, \quad \text{(A8)}$$

which does not contain the identity representation. Therefore there are no cubic terms contained within the primitive cell.

For $[\Gamma,L_a,L_a]$, we must execute the symmetric direct product of all full space group irreducible representations associated with each little group irreducible representation for each $\mathbf{q} \in Q$, which results in

$$\begin{aligned} &d_{\Gamma\ L_a\ L_a}^{T_{1u}A_{1g}A_{2u}}, \quad d_{\Gamma\ L_a\ L_a}^{T_{1u}A_{1g}E_u}, \quad d_{\Gamma\ L_a\ L_a}^{T_{1u}A_{2u}E_g}, \\ &{}^0d_{\Gamma\ L_aL_a}^{T_{1u}E_gE_u}, \quad {}^1d_{\Gamma\ L_aL_a}^{T_{1u}E_gE_u}. \end{aligned} \quad \text{(A9)}$$

where the left superscript indicates that multiple identity representations are produced in that product.

For $[L_a,L_b,X_z]$, we follow the same procedure, obtaining

$$\begin{aligned} &d_{L_b\ L_a\ X_z}^{A_{1g}A_{2u}A_{2u}}, \quad d_{L_b\ L_a\ X_z}^{A_{1g}A_{2u}{}^1A_{2u}}, \quad d_{L_b\ L_a\ X_z}^{A_{1g}A_{2u}E_u}, \quad d_{L_b\ L_a\ X_z}^{A_{1g}A_{2u}{}^1E_u}, \\ &d_{L_b\ L_aX_z}^{A_{1g}E_uA_{2u}}, \quad d_{L_b\ L_aX_z}^{A_{1g}E_u{}^1A_{2u}}, \quad {}^0d_{L_b\ L_aX_z}^{A_{1g}E_uE_u}, \quad {}^1d_{L_b\ L_aX_z}^{A_{1g}E_uE_u}, \\ &{}^0d_{L_b\ L_aX_z}^{A_{1g}E_u{}^1E_u}, \quad {}^1d_{L_b\ L_aX_z}^{A_{1g}E_u{}^1E_u}, \quad {}^0d_{L_b\ L_a\ X_z}^{E_gA_{2u}E_u}, \quad {}^1d_{L_b\ L_a\ X_z}^{E_gA_{2u}E_u}, \\ &{}^0d_{L_b\ L_a\ X_z}^{E_gA_{2u}{}^1E_u}, \quad {}^1d_{L_b\ L_a\ X_z}^{E_gA_{2u}{}^1E_u}, \quad {}^0d_{L_b\ L_aX_z}^{E_gE_uA_{2u}}, \quad {}^1d_{L_b\ L_aX_z}^{E_gE_uA_{2u}}, \\ &{}^0d_{L_b\ L_aX_z}^{E_gE_uE_u}, \quad {}^1d_{L_b\ L_aX_z}^{E_gE_uE_u}, \quad {}^2d_{L_b\ L_aX_z}^{E_gE_uE_u}, \quad {}^3d_{L_b\ L_aX_z}^{E_gE_uE_u}, \\ &{}^0d_{L_b\ L_aX_z}^{E_gE_u{}^1E_u}, \quad {}^1d_{L_b\ L_aX_z}^{E_gE_u{}^1E_u}, \quad {}^2d_{L_b\ L_aX_z}^{E_gE_u{}^1E_u}, \quad {}^3d_{L_b\ L_aX_z}^{E_gE_u{}^1E_u}, \\ &{}^0d_{L_b\ L_aX_z}^{E_gE_u{}^1A_{2u}}, \quad {}^1d_{L_b\ L_aX_z}^{E_gE_u{}^1A_{2u}}, \quad d_{L_b\ L_a\ X_z}^{E_gA_{2u}A_{2u}}, \quad d_{L_b\ L_a\ X_z}^{E_gA_{2u}{}^1A_{2u}}, \end{aligned} \quad \text{(A10)}$$

where the left superscripts of the irreducible representations indicate multiple instances of irreducible representations of displacements; the zeroth instance is not labeled.

The same analysis for $[\Gamma,X_z,X_z]$ and $[X_x,X_y,X_z]$ proves that there are no allowed derivatives in those two Q. In conclusion, there are a total of 33 space group irreducible derivatives. One can reach the same conclusion by inspecting the product and symmetric product tables, which were constructed to third order, for $Fm\bar{3}m$ by Birman *et al.* [94].

1. SS-BID and HS-BID approach with PD₁ for $\mathcal{N} = 3$ and $\hat{\mathbf{S}}_{\mathrm{BZ}} = 2\hat{\mathbf{1}}$

We begin by evaluating the SS-BID approach, where the maximum number of irreducible derivatives are measured simultaneously in the BvK supercell. In this case, we have $n_{ir}^{2\hat{\mathbf{1}}} = 33$ and $n_F^{2\hat{\mathbf{1}}} = 2^3 \cdot 6 - 3 = 45$, and therefore $n_m^{2\hat{\mathbf{1}}} \geqslant 1$, and explicit calculation confirms $n_m^{2\hat{\mathbf{1}}} = 1$ can be reached; meaning that all irreducible derivatives can be obtained in a single measurement.

However, it is clearly more efficient to avoid the BvK supercell altogether using the HS-BID approach. Using the Smith normal form of the two allowed Q, we can find the smallest supercells for each case:

$$\hat{\mathbf{S}}_{[\Gamma, L_a, L_a]} = \begin{bmatrix} 2 & 0 & 0 \\ 0 & 1 & 0 \\ 0 & 0 & 1 \end{bmatrix}, \quad \hat{\mathbf{S}}_{[L_a, L_b, X_z]} = \begin{bmatrix} 2 & 0 & 0 \\ 0 & 2 & 0 \\ 0 & 0 & 1 \end{bmatrix}. \tag{A11}$$

For $\hat{\mathbf{S}}_{[\Gamma, L_a, L_a]}$, there are $n_{ir}^{\vee \hat{\mathbf{S}}_{[\Gamma, L_a, L_a]}} = 5$ irreducible derivatives and there are $n_F^{\vee \hat{\mathbf{S}}_{[\Gamma, L_a, L_a]}} = 2 \cdot 6 - 3 = 9$ nonzero force equations, thus we have $n_m^{\vee \hat{\mathbf{S}}_{[\Gamma, L_a, L_a]}} \geqslant 1$; and explicit calculation confirms the equality can be realized. For $[L_a, L_b, X_z]$, there are $n_{ir}^{\vee \hat{\mathbf{S}}_{[L_a, L_b, X_z]}} = 28$ irreducible derivatives and there are $n_F^{\vee \hat{\mathbf{S}}_{[L_a, L_b, X_z]}} = 3 \cdot 6 = 18$ nonzero force equations, where we do not count the Γ-point optical modes as there are no derivatives with respect to the Γ being computed in this supercell; so we see that $n_m^{\vee \hat{\mathbf{S}}_{[L_a, L_b, X_z]}} \geqslant 2$, and explicit calculation confirms the equality can be realized.

Finally, we note that we can exploit overbundling in this situation, given that $\hat{\mathbf{S}}_{[L_a, L_b, X_z]}$ also accommodates $[\Gamma, L_a, L_a]$. In this scenario, we would have $n_{ir}^{\vee \hat{\mathbf{S}}_{[L_a, L_b, X_z]}} = 33$ and $n_F^{\hat{\mathbf{S}}_{[L_a, L_b, X_z]}} = 4 \cdot 6 - 3 = 21$; so $n_m^{\hat{\mathbf{S}}_{[L_a, L_b, X_z]}} \geqslant 2$ and explicit calculations confirm that all 33 irreducible derivatives can be obtained in two measurements. Therefore we obtain all five irreducible derivatives from $[\Gamma, L_a, L_a]$ at no extra cost.

APPENDIX B: PHONONS OF ZrO₂

In this section, we execute our method in the case of phonons of ZrO_2, comparing to the previously published work [11]. ZrO_2 has space group symmetry $Fm\bar{3}m$, and we study the FTG corresponding to the $2 \times 2 \times 2$ supercell of the conventional cubic unit cell. The primitive lattice cell vectors have the same form as rock salt, Eq. (A1), while the conventional cubic cell is

$$\hat{\mathbf{S}}_C = \begin{bmatrix} \bar{1} & 1 & 1 \\ 1 & \bar{1} & 1 \\ 1 & 1 & \bar{1} \end{bmatrix}. \tag{B1}$$

Therefore the BvK supercell is $\hat{\mathbf{S}}_{\mathrm{BZ}} = 2\hat{\mathbf{S}}_C$, and we have $n_q = \det(\hat{\mathbf{S}}_{\mathrm{BZ}}) = 32$. All of the conventions defined in rock salt will follow throughout. The irreducible set of $\tilde{q}_{\mathrm{BZ}}$ is given by

$$\tilde{q}_{\mathrm{IBZ}} = \{\Gamma, L, X, A, \Delta, W\}, \tag{B2}$$

where

$$\Gamma = (0, 0, 0), \quad L = \left(\tfrac{1}{2}, 0, 0\right), \quad X = \left(\tfrac{1}{2}, \tfrac{1}{2}, 0\right),$$
$$A = \left(\tfrac{1}{4}, \tfrac{3}{4}, 0\right), \quad \Delta = \left(\tfrac{1}{4}, \tfrac{1}{4}, 0\right), \quad W = \left(\tfrac{1}{4}, \tfrac{3}{4}, \tfrac{1}{2}\right). \tag{B3}$$

The irreducible representations of the displacements according to $\tilde{G}_{\mathbf{q}}$ are

$$\hat{\mathcal{U}}_\Gamma = (T_{2g}) \oplus T_{1u},$$
$$\hat{\mathcal{U}}_L = \left(A_{1g} \oplus {}^1A_{2u} \oplus E_g \oplus {}^1E_u\right)$$
$$\qquad \oplus (A_{2u} \oplus E_u),$$
$$\hat{\mathcal{U}}_X = \left(A_{1g} \oplus B_{1u} \oplus E_g \oplus {}^1E_u\right)$$
$$\qquad \oplus (A_{2u} \oplus E_u),$$
$$\hat{\mathcal{U}}_A = \left({}^1A_1 \oplus {}^2A_1 \oplus A_2 \oplus {}^1B_1 \oplus {}^2B_1 \oplus {}^1B_2\right)$$
$$\qquad \oplus (A_1 \oplus B_1 \oplus B_2),$$
$$\hat{\mathcal{U}}_\Delta = \left({}^1A_1 \oplus B_2 \oplus {}^1E \oplus {}^2E\right)$$
$$\qquad \oplus (A_1 \oplus E),$$
$$\hat{\mathcal{U}}_W = \left(A_1 \oplus A_2 \oplus {}^1B_1 \oplus B_2 \oplus {}^1E\right)$$
$$\qquad \oplus (B_1 \oplus E), \tag{B4}$$

where the first set of parenthesis enclose irreducible representations purely associated with O atoms, while the second set correspond purely to Zr. The T_{1u} mode, which is not enclosed in any parenthesis, is a mixture of Zr and O atoms. The left superscripts of the irreducible representations indicate multiple instances of irreducible representations of displacements; the zeroth instance is not labeled.

The number of irreducible derivatives can be determined by inspecting Eq. (B4), counting once for each irreducible representation and once for each pair of repeating irreducible representations at a given **q**:

$$n_{ir}^{\hat{\mathbf{S}}_{\mathrm{BZ}}} = \sum_{\mathbf{q} \in \tilde{q}_{\mathrm{IBZ}}, \alpha \in \mathcal{U}_{\mathbf{q}}} \frac{1}{2} a_{\mathbf{q}}^\alpha \left(a_{\mathbf{q}}^\alpha + 1\right). \tag{B5}$$

The above equation is applicable for $\mathcal{N} = 2$, where $\bar{\mathbf{q}} \in \tilde{s}_{\mathbf{q}} \forall \mathbf{q} \in \tilde{q}_{\mathrm{IBZ}}$, and in this case, it yields 52 irreducible derivatives. All 52 space group irreducible derivatives are listed in Table III, and they may be chosen to be real given the presence of inversion and time reversal symmetry. This proves that the analysis in Ref. [11] did not properly account for all symmetry, as they arrived at 59 nonzero parameters.

We now turn to extracting these 52 irreducible derivatives using SS-BID, and we can use the specific second-order equation for the number of measurements in Eq. (44). The result is that $n_m^{2\hat{\mathbf{S}}_C} = 1$, and all derivatives can be extracted from a single measurement; as compared to the two measurements (i.e., four calculations) in the original study [11]. We demonstrate the result of this single measurement, providing all space group irreducible derivatives in Table III, along with a plot of the phonons in Fig. 10.

The execution of the SS-BID is only a proof of principle, as in practice one would always perform HS-BID as

it is far more efficient. Indeed, HS-BID completely avoids the BvK supercell $\hat{\mathbf{S}}_{BZ} = 2\hat{\mathbf{S}}_C$, extracting all irreducible

$$\hat{\mathbf{S}}_\Gamma = \hat{1}, \quad \hat{\mathbf{S}}_L = \begin{bmatrix} 2 & 0 & 0 \\ 0 & 1 & 0 \\ 0 & 0 & 1 \end{bmatrix}, \quad \hat{\mathbf{S}}_X = \begin{bmatrix} 1 & 1 & 0 \\ 0 & 2 & 0 \\ 0 & 0 & 1 \end{bmatrix}, \quad \hat{\mathbf{S}}_A = \begin{bmatrix} 1 & 1 & 0 \\ 0 & 4 & 0 \\ 0 & 0 & 1 \end{bmatrix}, \quad \hat{\mathbf{S}}_\Delta = \begin{bmatrix} 2 & 2 & 0 \\ 1 & 3 & 0 \\ 0 & 0 & 1 \end{bmatrix}, \quad \hat{\mathbf{S}}_W = \begin{bmatrix} 2 & 0 & 1 \\ 1 & 1 & 0 \\ 0 & 0 & 2 \end{bmatrix}.$$

(B6)

The number of measurements required in each supercell is 1, 2, 1, 2, 1, and 1, respectively. The gain in time complexity as is described in Sec. III F is an order of magnitude. Furthermore, overbundling can be exploited, only requiring the supercells $\hat{\mathbf{S}}_L, \hat{\mathbf{S}}_A, \hat{\mathbf{S}}_\Delta, \hat{\mathbf{S}}_W$ with 2, 2, 1, and 1 measurements, respectively; eliminating the need for $\hat{\mathbf{S}}_X$ and $\hat{\mathbf{S}}_\Gamma$ entirely (see Table II for detailed comparison between different methods at $\mathcal{N} = 2$, and Ref. [15], Table SIV for similar comparison at $\mathcal{N} = 3$).

Density functional theory (DFT) calculations within the local density approximation (LDA) [16] were performed using the projector augmented wave (PAW) method [17,18], as implemented in the Vienna *ab initio* simulation package (VASP) [19–22]. A plane wave basis with a kinetic energy cutoff of 700 eV was employed. We used a Γ-centered **k**-point mesh of $4 \times 4 \times 4$. All k-point integrations were done using tetrahedron method with Blöchl corrections [98]. The crystal structure was relaxed, yielding a lattice parameter of 5.0303 Å.

APPENDIX C: EXAMPLE OF MINIMUM CELL FOR GIVEN $\mathcal{Q}$

Here we give an example illustrating how to find the minimum supercell that accommodates a given $\mathcal{Q}$ (see derivation and definitions in Sec. III B). There is no need to specify a
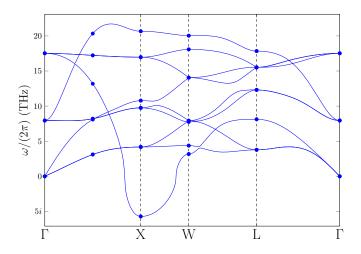

FIG. 10. Phonons of ZrO_2 within DFT for $\hat{\mathbf{S}}_{BZ} = 2\hat{\mathbf{S}}_C$, where data points are direct computational measurements and lines are Fourier interpolation of the measurements. The irreducible derivatives for $\hat{\mathbf{S}}_{BZ}$ are shown in Table III. When irreducible representations do not repeat at a given **q**, the phonon frequency is given by $\omega_\mathbf{q}^\alpha = \sqrt{d_{\mathbf{q}\mathbf{q}}^{\alpha\alpha}/m}$, where $m = m_i \cdot 1.0364 \times 10^{-28}$ eV s^2 Å^{-2}, with either $m_O = 15.9994$ or $m_{Zr} = 91.224$. The y axis plots $\omega_\mathbf{q}^\alpha \times 10^{-12}/(2\pi)$, giving units of terahertz (THz). LO-TO splitting has not been incorporated.

derivatives from smaller supercells. In this case, we have $\tilde{\mathbf{S}}_{BZ} = \{\hat{\mathbf{S}}_\Gamma, \hat{\mathbf{S}}_L, \hat{\mathbf{S}}_X, \hat{\mathbf{S}}_A, \hat{\mathbf{S}}_\Delta, \hat{\mathbf{S}}_W\}$, where

crystal structure given that this problem is only specific to the translation group. Let us consider an example for $\mathcal{N} = 3$:

$$\mathcal{Q} = \left(\left(\tfrac{1}{4}, \tfrac{3}{4}, \tfrac{1}{2}\right), \left(\tfrac{1}{4}, \tfrac{1}{4}, 0\right), \left(\tfrac{1}{2}, 0, \tfrac{1}{2}\right)\right). \quad (C1)$$

Here, $L = 4$, and we can now drop the third row of $\hat{\mathcal{Q}}$, for example, and multiply $\hat{\mathcal{Q}}$ by L to obtain $\hat{\mathcal{Q}}'$:

$$\hat{\mathcal{Q}}' = \begin{bmatrix} 1 & 3 & 2 \\ 1 & 1 & 0 \end{bmatrix}. \quad (C2)$$

We can apply row and column operations $\hat{\mathbf{R}}$ and $\hat{\mathbf{C}}$ in order to achieve the Smith normal form $\hat{\mathbf{N}} = \hat{\mathbf{R}}\hat{\mathcal{Q}}'\hat{\mathbf{C}}$:

$$\hat{\mathbf{N}} = \begin{bmatrix} 1 & 0 & 0 \\ 0 & 2 & 0 \end{bmatrix}, \quad \hat{\mathbf{R}} = \begin{bmatrix} 0 & 1 \\ 1 & -1 \end{bmatrix}, \quad \hat{\mathbf{C}} = \begin{bmatrix} 1 & -1 & 1 \\ 0 & 1 & -1 \\ 0 & 0 & 1 \end{bmatrix}.$$

(C3)

It is straightforward to write the kernel of $\hat{\mathbf{N}}$, according to Eq. (33):

$$\ker(\hat{\mathbf{N}}) = \begin{bmatrix} 4 & 0 & 0 \\ 0 & 2 & 0 \\ 0 & 0 & 1 \end{bmatrix}. \quad (C4)$$

Finally, the kernel of $\hat{\mathcal{Q}}'$ can be easily constructed, in addition to a minimal supercell which accommodates $\mathcal{Q}$:

$$\ker(\hat{\mathcal{Q}}') = \hat{\mathbf{C}} \ker(\hat{\mathbf{N}}) = \begin{bmatrix} 4 & -2 & 1 \\ 0 & 2 & -1 \\ 0 & 0 & 1 \end{bmatrix} = \hat{\mathbf{S}}_\mathcal{Q}^\mathsf{T}. \quad (C5)$$

TABLE II. Required calculations for ZrO_2 at $\mathcal{N} = 2$ with $\hat{\mathbf{S}}_{BZ} = 2\hat{\mathbf{S}}_C$ in different methods. In the HS-BID method, overbundling can be employed to reduce calculations, and paranthesis indicate the overbundled quantities. The number of DFT calculations is n_{DFT}.

Method	**q**	$\hat{\mathbf{S}}$	$\det(\hat{\mathbf{S}})$	$n_m^{\hat{\mathbf{S}}}$	n_{DFT}
SS-BID		$2\hat{\mathbf{S}}_C$	32	1	2
HS-BID	$L, (\Gamma)$	$\hat{\mathbf{S}}_L(\hat{\mathbf{S}}_\Gamma)$	2	2 (1)	4 (2)
	$A, (X)$	$\hat{\mathbf{S}}_A(\hat{\mathbf{S}}_X)$	4	2 (1)	4 (2)
	Δ	$\hat{\mathbf{S}}_\Delta$	4	1	2
	W	$\hat{\mathbf{S}}_W$	4	1	2
HS-LID	Γ	$\hat{\mathbf{S}}_\Gamma$	1	2	4
	L	$\hat{\mathbf{S}}_L$	2	6	12
	X	$\hat{\mathbf{S}}_X$	2	6	12
	A	$\hat{\mathbf{S}}_A$	4	9	18
	Δ	$\hat{\mathbf{S}}_\Delta$	4	6	12
	W	$\hat{\mathbf{S}}_W$	4	7	14

TABLE III. Irreducible derivatives of ZrO_2 for $\mathcal{N} = 2$ and $\hat{\mathbf{S}}_{\mathrm{BZ}} = 2\hat{\mathbf{S}}_C$ in units of eV/Å^2.

Derivative	Value	Derivative	Value
$d_{\Gamma\ \Gamma}^{T_{2g} T_{2g}}$	20.105	$d_{\Gamma\ \Gamma}^{T_{1u} T_{1u}}$	9.189
$d_{L\ L}^{A_{1g} A_{1g}}$	20.828	$d_{L\ L}^{E_g E_g}$	15.766
$d_{L\ L}^{A_{2u} A_{2u}}$	33.220	$d_{L\ L}^{A_{2u} {}^1A_{2u}}$	−9.242
$d_{L\ L}^{{}^1A_{2u} {}^1A_{2u}}$	14.278	$d_{L\ L}^{E_u E_u}$	5.937
$d_{L\ L}^{E_u {}^1E_u}$	−2.346	$d_{L\ L}^{{}^1E_u {}^1E_u}$	9.819
$d_{X\ X}^{A_{1g} A_{1g}}$	27.957	$d_{X\ X}^{E_g E_g}$	6.221
$d_{X\ X}^{A_{2u} A_{2u}}$	43.374	$d_{X\ X}^{B_{1u} B_{1u}}$	−2.139
$d_{X\ X}^{E_u E_u}$	6.614	$d_{X\ X}^{E_u {}^1E_u}$	−1.339
$d_{X\ X}^{{}^1E_u {}^1E_u}$	18.834		
$d_{\bar{A}\ A}^{A_1 A_1}$	30.934	$d_{\bar{A}\ A}^{{}^1A_1 {}^1A_1}$	4.000
$d_{\bar{A}\ A}^{A_1 {}^2A_1}$	−10.720	$d_{\bar{A}\ A}^{{}^1A_1 {}^1A_1}$	22.021
$d_{\bar{A}\ A}^{{}^1A_1 {}^2A_1}$	−1.691	$d_{\bar{A}\ A}^{{}^2A_1 {}^2A_1}$	21.250
$d_{\bar{A}\ A}^{B_2 B_2}$	6.135	$d_{\bar{A}\ A}^{B_2 {}^1B_2}$	−2.558
$d_{\bar{A}\ A}^{B_1 {}^1B_1}$	2.580	$d_{\bar{A}\ A}^{{}^1B_2 {}^1B_2}$	12.342
$d_{\bar{A}\ A}^{{}^1B_1 {}^2B_1}$	−1.515	$d_{\bar{A}\ A}^{{}^2B_1 {}^2B_1}$	10.480
$d_{\bar{A}\ A}^{A_2 A_2}$	13.783	$d_{\bar{A}\ A}^{B_1 B_1}$	13.532
$d_{\bar{A}\ A}^{B_1 {}^1B_1}$	−2.990	$d_{\bar{A}\ A}^{{}^1B_1 {}^1B_1}$	3.481
$d_{\bar{\Delta}\ \Delta}^{A_1 A_1}$	41.658	$d_{\bar{\Delta}\ \Delta}^{A_1 {}^1A_1}$	−18.449
$d_{\bar{\Delta}\ \Delta}^{{}^1A_1 {}^1A_1}$	24.050	$d_{\bar{\Delta}\ \Delta}^{B_2 B_2}$	11.378
$d_{\bar{\Delta}\ \Delta}^{E E}$	6.380	$d_{\bar{\Delta}\ \Delta}^{E {}^1E}$	−2.896
$d_{\bar{\Delta}\ \Delta}^{E {}^2E}$	0.918	$d_{\bar{\Delta}\ \Delta}^{{}^1E {}^1E}$	4.395
$d_{\bar{\Delta}\ \Delta}^{{}^1E {}^2E}$	2.673	$d_{\bar{\Delta}\ \Delta}^{{}^2E {}^2E}$	18.958
$d_{\bar{W}\ W}^{A_1 A_1}$	26.263	$d_{\bar{W}\ W}^{B_1 B_1}$	7.193
$d_{\bar{W}\ W}^{B_1 B_1}$	0.973	$d_{\bar{W}\ W}^{{}^1B_1 {}^1B_1}$	21.398
$d_{\bar{W}\ W}^{A_2 A_2}$	0.659	$d_{\bar{W}\ W}^{B_2 B_2}$	3.936
$d_{\bar{W}\ W}^{E E}$	23.596	$d_{\bar{W}\ W}^{E {}^1E}$	1.211
$d_{\bar{W}\ W}^{{}^1E {}^1E}$	12.905		

We emphasize that this particular choice of supercell is not unique, and may be reshaped.

APPENDIX D: AN EFFICIENT ALGORITHM TO CONSTRUCT $\tilde{t}_{\mathrm{BZ}}$ FOR A GIVEN $\hat{\mathbf{S}}_{\mathrm{BZ}}$

Here we present an efficient algorithm to solve Eq. (7) for the set $\tilde{t}_{\mathrm{BZ}}$ given $\hat{\mathbf{S}}_{\mathrm{BZ}}$. The same algorithm can be applied to Eq. (8), since the two equations have similar form. Recall Eq. (7)

$$0 \leqslant \mathbf{t}\hat{\mathbf{S}}_{\mathrm{BZ}}^{-1} \cdot \mathbf{e}_j < 1 \quad \text{for} \quad j = 1, \ldots, d, \quad (D1)$$

where $\mathbf{e}_j$ is a unit vector in $\mathbb{Z}^d$.

Given that $\hat{\mathbf{S}}_{\mathrm{BZ}}$ is an integer matrix, we can construct the column-style Hermite norm form [86], which is a lower triangular matrix $\hat{\mathbf{H}}$, via integer column transformations $\hat{\mathbf{U}}$ (here $\hat{\mathbf{U}}$ and $\hat{\mathbf{U}}^{-1}$ are both unimodular integer matrices): $\hat{\mathbf{H}} = \hat{\mathbf{S}}_{\mathrm{BZ}}\hat{\mathbf{U}}$; and this form can be used to rewrite Eq. (D1):

$$0 \leqslant \mathbf{t}\hat{\mathbf{U}}\hat{\mathbf{H}}^{-1} \cdot \mathbf{e}_j < 1 \quad \text{for} \quad j = 1, \ldots, d,$$
$$0 \leqslant \mathbf{t}'\hat{\mathbf{H}}^{-1} \cdot \mathbf{e}_j < 1, \quad (D2)$$

where $\mathbf{t}' = \mathbf{t}\hat{\mathbf{U}}$ is an integer vector, given that $\mathbf{t}$ is an integer vector, and $\hat{\mathbf{H}}^{-1}$ is a lower triangular matrix:

$$\hat{\mathbf{H}}^{-1} = \begin{bmatrix} H_{11}^i & 0 & \cdots & 0 \\ H_{21}^i & H_{22}^i & \cdots & 0 \\ \vdots & \vdots & \ddots & \vdots \\ H_{d1}^i & H_{d2}^i & \cdots & H_{dd}^i \end{bmatrix}, \quad (D3)$$

where H_{ij}^i are the matrix elements of $\hat{\mathbf{H}}^{-1}$.

If we take an example of $d = 3$, then we have

$$0 \leqslant t_1' H_{11}^i + t_2' H_{21}^i + t_3' H_{31}^i < 1,$$
$$0 \leqslant t_2' H_{22}^i + t_3' H_{32}^i < 1, \quad (D4)$$
$$0 \leqslant t_3' H_{33}^i < 1,$$

where t_i' are the components of $\mathbf{t}'$. The linear equations can easily be solved from the bottom to the top for all $\mathbf{t}'$, and then $\mathbf{t} = \mathbf{t}'\hat{\mathbf{U}}^{-1}$.

[1] M. T. Dove, *Introduction to Lattice Dynamics* (Cambridge University Press, Cambridge, 1993).

[2] G. Srivastava, *The Physics of Phonons* (CRC Press, Bristol, England, 1990).

[3] J. A. Reissland, *The Physics of Phonons* (Wiley-Interscience, London, 1973).

[4] B. Fultz, Prog. Mater. Sci. **55**, 247 (2010).

[5] A. van de Walle and G. Ceder, Rev. Mod. Phys. **74**, 11 (2002).

[6] R. M. Martin, *Electronic Structure: Basic Theory and Practical Methods* (Cambridge University Press, Cambridge, 2004).

[7] S. Baroni, S. de Gironcoli, A. Dal Corso, and P. Giannozzi, Rev. Mod. Phys. **73**, 515 (2001).

[8] J. Ihm, M. Yin, and M. L. Cohen, Solid State Commun. **37**, 491 (1981).

[9] N. Bonini, M. Lazzeri, N. Marzari, and F. Mauri, Phys. Rev. Lett. **99**, 176802 (2007).

[10] P. Giannozzi, S. de Gironcoli, P. Pavone, and S. Baroni, Phys. Rev. B **43**, 7231 (1991).

[11] K. Parlinski, Z. Q. Li, and Y. Kawazoe, Phys. Rev. Lett. **78**, 4063 (1997).

[12] G. P. Zhang and T. F. George, Phys. Rev. B **69**, 167102 (2004).

[13] A. Floris, S. de Gironcoli, E. K. U. Gross, and M. Cococcioni, Phys. Rev. B **84**, 161102(R) (2011).

[14] B. Dorado, J. Bieder, and M. Torrent, J. Phys.: Condens. Matter **29**, 245402 (2017).

[15] See Supplemental Material at http://link.aps.org/supplemental/10.1103/PhysRevB.100.014303 for a glossary of key variables; additional figures of Grüneisen parameters, quadratic error tails, and strain derivatives of phonons; tables of symmetrized displacement amplitudes, irreducible derivatives of graphene for third order, and cost analysis on ZrO_2 at third order .

[16] J. P. Perdew and A. Zunger, Phys. Rev. B **23**, 5048 (1981).

[17] P. E. Blöchl, Phys. Rev. B **50**, 17953 (1994).

[18] G. Kresse and D. Joubert, Phys. Rev. B **59**, 1758 (1999).

[19] G. Kresse and J. Hafner, Phys. Rev. B **47**, 558 (1993).

[20] G. Kresse and J. Hafner, Phys. Rev. B **49**, 14251 (1994).

[21] G. Kresse and J. Fürthmuller, Comput. Mater. Sci. **6**, 15 (1996).

[22] G. Kresse and J. Fürthmuller, Phys. Rev. B **54**, 11169 (1996).

[23] J. F. Cornwell, *Group Theory In Physics* (Academic Press, London, 1997).

[24] A. Zee, *Group Theory in a Nutshell for Physicists* (Princeton University Press, Princeton, New Jersey, 2016).

[25] J. J. Sakurai, *Modern Quantum Mechanics* (Addison Wesley, Reading, Massachusetts, 1993).

[26] W. Greiner and J. Maruhn, *Nuclear Models* (Springer, Berlin, 1996).

[27] M. Tinkham, *Group Theory And Quantum Mechanics* (Courier Corporation, Mineola, New York, 2012).

[28] A. P. Cracknell and B. L. Davies, *Kronecker Product Tables* (IFI/Plenum, New York, 1980).

[29] J. L. Birman, Phys. Rev. **127**, 1093 (1962).

[30] M. Lax, Phys. Rev. **138**, A793 (1965).

[31] J. L. Birman, Phys. Rev. **150**, 771 (1966).

[32] J. Zak, Phys. Rev. **151**, 464 (1966).

[33] D. H. Lewis, J. Phys. A **6**, 125 (1973).

[34] P. Gard, J. Phys. A **6**, 1807 (1973).

[35] P. Gard, J. Phys. A **6**, 1829 (1973).

[36] J. L. Birman, *Theory of Crystal Space Groups and Lattice Dynamics: Infra-Red and Raman Optical Processes of Insulating Crystals* (Springer, Berlin, 1984).

[37] J. C. Tolédano and P. Tolédano, *Landau Theory Of Phase Transitions, The: Application To Structural, Incommensurate, Magnetic And Liquid Crystal Systems* (World Scientific Publishing Company, Singapore, 1987).

[38] M. Born and K. Huang, *Dynamical Theory Of Crystal Lattices* (Oxford University Press, Oxford, 1998).

[39] G. Leibfried and W. Ludwig, in *Solid State Physics* (Elsevier, 1961), pp. 275–444.

[40] G. K. Horton and A. A. Maradudin, *Dynamical Properties of Solids: Crystalline Solids, Fundamentals* (North-Holland, Amsterdam, 1974).

[41] D. Alfè, Comput. Phys. Commun. **180**, 2622 (2009).

[42] Y. Wang, L.-Q. Chen, and Z.-K. Liu, Comput. Phys. Commun. **185**, 2950 (2014).

[43] A. Togo and I. Tanaka, Scripta Materialia **108**, 1 (2015).

[44] K. Esfarjani and H. T. Stokes, Phys. Rev. B **77**, 144112 (2008).

[45] L. Chaput, A. Togo, I. Tanaka, and G. Hug, Phys. Rev. B **84**, 094302 (2011).

[46] O. Hellman and I. A. Abrikosov, Phys. Rev. B **88**, 144301 (2013).

[47] F. Zhou, W. Nielson, Y. Xia, and V. Ozoliņš, Phys. Rev. Lett. **113**, 185501 (2014).

[48] K. H. Ahn, T. Lookman, A. Saxena, and A. R. Bishop, Phys. Rev. B **68**, 092101 (2003).

[49] K. H. Ahn, T. Lookman, and A. R. Bishop, Nature (London) **428**, 401 (2004).

[50] T. F. Seman, J. Moon, and K. H. Ahn, Emerging Mater. Res. **2**, 5 (2013).

[51] X. Ai, Y. Chen, and C. A. Marianetti, Phys. Rev. B **90**, 014308 (2014).

[52] M. Kornbluth, Ph.D. thesis, Columbia University, 2017.

[53] J. C. Thomas and A. Van der Ven, Phys. Rev. B **88**, 214111 (2013).

[54] I. Leonov, V. I. Anisimov, and D. Vollhardt, Phys. Rev. Lett. **112**, 146401 (2014).

[55] K. Haule and G. L. Pascut, Phys. Rev. B **94**, 195146 (2016).

[56] E. N. Zein, Fiz. Tverd. Tela (Leningrad) **26**, 3024 (1984) [Sov. Phys. Solid State **26**, 1825 (1984)].

[57] S. Baroni, P. Giannozzi, and A. Testa, Phys. Rev. Lett. **58**, 1861 (1987).

[58] X. Gonze and J.-P. Vigneron, Phys. Rev. B **39**, 13120 (1989).

[59] X. Gonze, Phys. Rev. A **52**, 1096 (1995).

[60] A. Debernardi, S. Baroni, and E. Molinari, Phys. Rev. Lett. **75**, 1819 (1995).

[61] M. Lazzeri and S. de Gironcoli, Phys. Rev. B **65**, 245402 (2002).

[62] L. Paulatto, F. Mauri, and M. Lazzeri, Phys. Rev. B **87**, 214303 (2013).

[63] G. Deinzer, G. Birner, and D. Strauch, Phys. Rev. B **67**, 144304 (2003).

[64] G. Fugallo, M. Lazzeri, L. Paulatto, and F. Mauri, Phys. Rev. B **88**, 045430 (2013).

[65] L. Paulatto, I. Errea, M. Calandra, and F. Mauri, Phys. Rev. B **91**, 054304 (2015).

[66] D. Campi, L. Paulatto, G. Fugallo, F. Mauri, and M. Bernasconi, Phys. Rev. B **95**, 024311 (2017).

[67] M. Markov, J. Sjakste, G. Fugallo, L. Paulatto, M. Lazzeri, F. Mauri, and N. Vast, Phys. Rev. B **93**, 064301 (2016).

[68] P. Giannozzi, O. Andreussi, T. Brumme, O. Bunau, M. B. Nardelli, M. Calandra, R. Car, C. Cavazzoni, D. Ceresoli, M. Cococcioni, N. Colonna, I. Carnimeo, A. D. Corso, S. de Gironcoli, P. Delugas, R. A. DiStasio, A. Ferretti, A. Floris, G. Fratesi, G. Fugallo, R. Gebauer, U. Gerstmann, F. Giustino, T. Gorni, J. Jia, M. Kawamura, H.-Y. Ko, A. Kokalj, E. Küçükbenli, M. Lazzeri, M. Marsili, N. Marzari, F. Mauri, N. L. Nguyen, H.-V. Nguyen, A. Otero-de-la-Roza, L. Paulatto, S. Poncé, D. Rocca, R. Sabatini, B. Santra, M. Schlipf, A. P. Seitsonen, A. Smogunov, I. Timrov, T. Thonhauser, P. Umari, N. Vast, X. Wu, and S. Baroni, J. Phys.: Condens. Matter **29**, 465901 (2017).

[69] P. Giannozzi, S. Baroni, N. Bonini, M. Calandra, R. Car, C. Cavazzoni, D. Ceresoli, G. L. Chiarotti, M. Cococcioni, I. Dabo, A. D. Corso, S. de Gironcoli, S. Fabris, G. Fratesi, R. Gebauer, U. Gerstmann, C. Gougoussis, A. Kokalj, M. Lazzeri, L. Martin-Samos, N. Marzari, F. Mauri, R. Mazzarello, S. Paolini, A. Pasquarello, L. Paulatto, C. Sbraccia, S. Scandolo, G. Sclauzero, A. P. Seitsonen, A. Smogunov, P. Umari, and

R. M. Wentzcovitch, J. Phys.: Condens. Matter **21**, 395502 (2009).

[70] H. Wendel and R. M. Martin, Phys. Rev. Lett. **40**, 950 (1978).

[71] M. T. Yin and M. L. Cohen, Phys. Rev. Lett. **45**, 1004 (1980).

[72] K. Kunc and R. M. Martin, Phys. Rev. B **24**, 2311 (1981).

[73] R. M. Martin, J. Phys. (Paris) Colloq. **42**, C6-617 (1981).

[74] K. Kunc and R. M. Martin, Phys. Rev. Lett. **48**, 406 (1982).

[75] W. Frank, C. Elsässer, and M. Fähnle, Phys. Rev. Lett. **74**, 1791 (1995).

[76] J. H. Lloyd-Williams and B. Monserrat, Phys. Rev. B **92**, 184301 (2015).

[77] D. Vanderbilt, S. H. Taole, and S. Narasimhan, Phys. Rev. B **40**, 5657 (1989).

[78] S. Narasimhan and D. Vanderbilt, Phys. Rev. B **43**, 4541 (1991).

[79] K. Esfarjani, G. Chen, and H. T. Stokes, Phys. Rev. B **84**, 085204 (2011).

[80] J. Shiomi, K. Esfarjani, and G. Chen, Phys. Rev. B **84**, 104302 (2011).

[81] Z. Tian, K. Esfarjani, J. Shiomi, A. S. Henry, and G. Chen, Appl. Phys. Lett. **99**, 053122 (2011).

[82] S. Lee, K. Esfarjani, J. Mendoza, M. S. Dresselhaus, and G. Chen, Phys. Rev. B **89**, 085206 (2014).

[83] L. Lindsay, D. A. Broido, and T. L. Reinecke, Phys. Rev. Lett. **109**, 095901 (2012).

[84] W. Li, J. Carrete, N. A. Katcho, and N. Mingo, Comput. Phys. Commun. **185**, 1747 (2014).

[85] J. J. Plata, P. Nath, D. Usanmaz, J. Carrete, C. Toher, M. de Jong, M. Asta, M. Fornari, M. B. Nardelli, and S. Curtarolo, npj Computational Materials **3**, 45 (2017).

[86] H. Cohen, *A Course in Computational Algebraic Number Theory* (Springer, Dordrecht, 1993).

[87] X.-F. Zhou and P. Pulay, J. Comput. Chem. **10**, 935 (1989).

[88] G. Lyubarskii, *The Application of Group Theory in Physics* (Elsevier, New York, 2013).

[89] M. Heideman, D. Johnson, and C. Burrus, IEEE ASSP Magazine **1**, 14 (1984).

[90] D.-B. Zhang, T. Sun, and R. M. Wentzcovitch, Phys. Rev. Lett. **112**, 058501 (2014).

[91] C. Norman, *Finitely Generated Abelian Groups and Similarity of Matrices over a Field* (Springer Science & Business Media, London, 2012).

[92] G. L. W. Hart and R. W. Forcade, Phys. Rev. B **77**, 224115 (2008).

[93] A. Togo, L. Chaput, and I. Tanaka, Phys. Rev. B **91**, 094306 (2015).

[94] L.-C. Chen, R. Berenson, and J. L. Birman, Phys. Rev. **170**, 639 (1968).

[95] D. C. Wallace, *Thermodynamics of Crystals* (Courier Corporation, New York, 1998).

[96] J. Fabian and P. B. Allen, Phys. Rev. Lett. **79**, 1885 (1997).

[97] C. H. Lee and C. K. Gan, Phys. Rev. B **96**, 035105 (2017).

[98] P. E. Blöchl, O. Jepsen, and O. K. Andersen, Phys. Rev. B **49**, 16223 (1994).